Journal of Sound and Vibration (1998) **214**(4), 605–637
Article No. sv981556

DYNAMIC ANALYSIS AND VIBRATION CONTROL OF A FLEXIBLE SLIDER–CRANK MECHANISM USING PM SYNCHRONOUS SERVO MOTOR DRIVE

R.-F. Fung and K.-W. Chen

Department of Mechanical Engineering, *Chung Yuan Christian University*, *Chung-Li*, *Taiwan* 32023, *Republic of China*

(*Received* 26 *May* 1997, *and in final form* 2 *January* 1998)

Dynamic analysis and vibration control of a flexible slider–crank mechanism driven by a permanent magnet (PM) synchronous servo motor are studied in this paper. Geometric constraint at the end of a flexible connecting rod is derived and introduced into Hamilton's principle to formulate the governing equations of the connecting rod which is modelled by Timoshenko beam theory. The coupling equations describe the rigid-body motion, flexible vibrations and motor system. In order to control crank speed and reduce flexible vibrations simultaneously, speed and tracking controllers are designed through a reaching law variable structure control (VSC) method. By choosing proper parameters in control law, dynamic responses of the flexible system in reaching mode can be controlled. Numerical results show that the proposed controllers not only eliminate the dynamic deflections of the flexible connecting rod, but also keep good tracking performances. Moreover, the robustness against external disturbances can also be improved by employing the proposed control scheme.

1. INTRODUCTION

The need for higher manufacturing throughput has led to the design of machines operating at higher speeds. Because of the higher operating speeds, mechanisms have been made as lightweight as possible to reduce the inertial forces and the driving torque requirements. At higher speeds, the rigid-body assumption is no longer valid and the links should be considered flexible. In addition, motor drives used to control the motion of a variety of machines usually contain flexible coupling. High-speed operations of these machines lead to deflections which affect the dynamic behaviour and the accuracy of the machines.

The slider–crank mechanism is widely used in gasoline and diesel engines, where the gas force acts on the slider and the motion is transmitted through the links. Earlier research work in analysis of elastic mechanisms can be found in many publications. Steady state solutions and the elastic stability of a slider–crank mechanism were obtained [1–5]. Transient responses were investigated by Chu and Pan [6] on the basis of the ratios of the length of the crank to that of the connecting rod, and rotating speeds of the crank to those of the rod, etc. Sadler and Sandor [7] developed a method of kineto-elastodynamic analysis by using lumped parameter models to simulate the moving components. Lieh [8] investigated the dynamic behaviour of a slider–crank mechanism with the flexible coupler and joint. However, the equations were linearized based on the small deformation

0022–460X/98/290605 + 33 $30.00/0

assumption. Fung [9] described the dynamic analysis of a slider–crank mechanism with the flexible connecting rod which is modelled by Timoshenko beam theory.

The dynamic analysis of a slider–crank mechanism has been studied extensively over the past 30 years, with much of the research going beyond the current paper to include a totally flexible mechanism. Wu and Mani [10] introduced the modelling of flexible bodies for multibody dynamic systems by using the Ritz vector. Liu and Lin [11] developed a finite element method based on the dynamic stiffness to investigate forced vibrations of a flexible system. Fallahi *et al*. [12] also developed a finite element formulation to analyze a flexible slider–crank mechanism system in which the local co-ordinate system was employed. A co-rotational finite element formulation of a slender curve beam element was presented by Hsiao and Yang [13]. Fung and Chen [14] presented a finite element method for the dynamic analysis of a flexible connecting rod of slider–crank mechanism with time-dependent boundary condition. In all the above references, the crank rotates with a constant speed. However, the realistic operating condition is that as the crank is driven by a PM synchronous servo motor, the rotation speed of the crank is not constant.

The computed torque method originally developed for rigid manipulators was tried on the flexible link systems [15]. In order to assure system robustness, Flcola *et al*. [16] presented a simplified strategy to implement the sliding mode control of a two-joint robot with a flexible forearm. Choi *et al*. [17] applied a new sliding mode controller to the tip position control of a single-link flexible manipulator. In recent years, advancements in magnetic materials, semiconductor power devices, and control theory have made the PM synchronous servo motor drive play a vitally important role in motion-control applications in the low-to-medium power range. The desirable features of the PM synchronous servo motor are its compact structure, high air-gap flux density, high power density, high torque-to-inertia ratio, and high torque capability. Moreover, compared with an induction servo motor, a PM synchronous servo motor has such advantages as higher efficiency, due to the absence of rotor losses and lower no-load current below the rated speed; and its decoupling control performance is much less sensitive to the parametric variation of the motor [18]. To achieve fast four-quadrant operation and smooth starting and acceleration, the field-oriented control [19], or vector control, is used in the design of the PM synchronous servo motor drive.

As far as the mechanism is concerned, little work has appeared on the coupled system, both from the point of view of the theoretical formulation of the problem and the vibration control of the mechanism behaviour. In this paper, the main objective is focused on the dynamic formulations and the vibration control of a PM synchronous servo motor coupled with a slider–crank mechanism system. First, a slider–crank mechanism system actuated by a PM synchronous servo motor is formulated. Next, in order to control the coupled mechanical system with robust characteristics, a variable structure controller is designed to control the crank with a constant angular speed and the desired trajectories. In addition, the problem of vibration control is addressed by substituting a saturation function for the control law. Numerical results show that the dynamic behaviour of the controller–motor–mechanism system not only reduces the dynamic deflections of the flexible connecting rod, but also keeps good tracking performances. In addition, it is also found that the proposed VSC is robust to external disturbances.

2. FORMULATION OF THE DYNAMIC MODEL

In this paper, the connecting rod is modelled as a Timoshenko beam, that is, the effects of rotary inertia and shear deformation are considered. The dynamic analysis process of the Euler-beam, simple-flexure and rigid-body models was given in reference [9] and a

constant rotation speed was assumed. However, in this paper the driven motor operates with non-constant speeds and the tracking trajectories. The flexible slider–crank mechanism driven by a PM synchronous servo motor is shown in Figure 1, and consists of the rigid crank OA with length r; the flexible cylindrical rod AB with length l; and the piston with mass M_4. For other symbols in this figure, see Nomenclature (Appendix E).

2.1. GOVERNING EQUATIONS

By using Hamilton's principle, integration by parts and some algebraic relations, a complete derivation of the equations of motion is given in Appendix A. The non-linear dynamic equations of motion are

$$\int_0^l -\rho A r\{r\theta_{tt} - [u_{tt} + v\phi_{tt} + 2v_t\,\phi_t - (x+u)\phi_t^2]\sin(\theta+\phi)$$
$$+[v_{tt} - (x+u)\phi_{tt} - 2u_t\,\phi_t - \phi_t^2\,u]\cos(\theta+\phi)\}\,\mathrm{d}x$$
$$-M_4\,r\{r\theta_{tt} - [u_{tt} + v\phi_{tt} + 2v_t\,\phi_t - (l+u)\phi_t^2]\sin(\theta+\phi)$$
$$+[v_{tt} - (l+u)\phi_{tt} - 2u_t\,\phi_t - \phi_t^2\,u]\cos(\theta+\phi)\} + \lambda r\cos\theta$$
$$-\tfrac{1}{3}M_2\,r^2\theta_{tt} + g_r\,K_t\,i_q^* - g_r^2\,J_m\,\theta_{tt} - g_r^2\,B_m\,\theta_t = 0, \tag{1a}$$

$$\int_0^l \{\rho A\{[r\theta_{tt}\sin(\theta+\phi) + r\theta_t^2\cos(\theta+\phi) - u_{tt} - 2v_t\,\phi_t - v\phi_{tt}]v$$
$$+(x+u)\,[r\theta_{tt}\cos(\theta+\phi) - r\theta_t^2\sin(\theta+\phi) + v_{tt} - 2u_t\,\phi_t - (x+u)\phi_{tt}]\}$$
$$+\rho I(\phi_{tt} - \psi_{tt} + \phi_{tt}\,\psi^2 + 2\phi_t\,\psi_t\,\psi)\}\,\mathrm{d}x$$
$$+M_4\,\{[r\theta_{tt}\sin(\theta+\phi) + r\theta_t^2\cos(\theta+\phi) - u_{tt} - 2v_t\,\phi_t - v\phi_{tt}]v$$
$$+(l+u)\,[r\theta_{tt}\cos(\theta+\phi) - r\theta_t^2\sin(\theta+\phi) + v_{tt} - 2u_t\,\phi_t - (l+u)\phi_{tt}]\}$$
$$-\lambda l\cos\phi - \{EAv_x\,(u_x + \tfrac{1}{2}v_x^2) + KGA(v_x - \psi) + M_4\,[r\theta_{tt}\cos(\theta+\phi)$$
$$-r\theta_t^2\sin(\theta+\phi) - 2\phi_t\,u_t - v\phi_t^2 + v_{tt} - (l+u)\phi_{tt}]\}u(l,t)\sec^2\phi = 0, \tag{1b}$$

$$\rho A[r\theta_t^2\cos(\theta+\phi) - 2v_t\,\phi_t + (x+u)\phi_t^2 + r\theta_{tt}\sin(\theta+\phi) - u_{tt} - v\phi_{tt}]$$
$$-C_x\,u_t + EA(u_{xx} + v_x\,v_{xx}) = 0, \tag{1c}$$

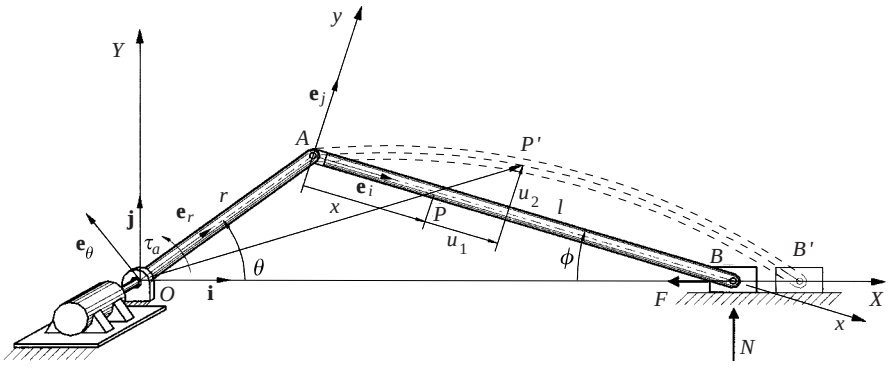

Figure 1. Slider–crank mechanism with a flexible connecting rod driven by a PM synchronous servo motor.

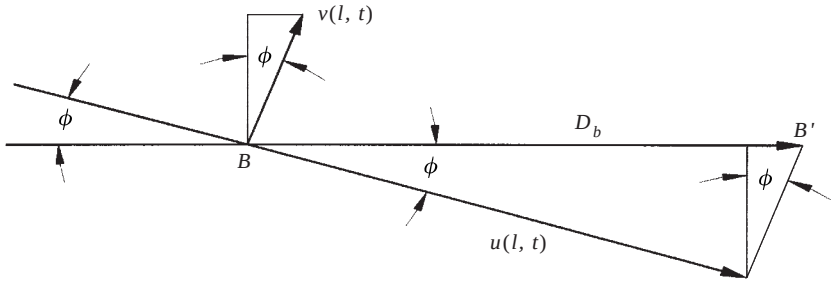

Figure 2. At end point B, the displacement relationship among D_b, $U(1, \tau)$ and $V(1, \tau)$.

$$\rho A[-r\theta_{tt}\cos(\theta+\phi)+r\theta_t^2\sin(\theta+\phi)+2\phi_t u_t+v\phi_t^2-v_{tt}+(x+u)\phi_{tt}]$$
$$-C_y v_t+EA[v_x(u_{xx}+v_x v_{xx})+v_{xx}(u_x+\tfrac{1}{2}v_x^2)]+KGA(v_{xx}-\psi_x)=0, \quad (1d)$$
$$\rho I(\phi_t^2\psi+\phi_{tt}-\psi_{tt})-C_\psi\psi_t+KGA(v_x-\psi)+EI\psi_{xx}=0, \quad (1e)$$

and the boundary conditions are

$$u(0,t)=0, \qquad v(0,t)=0, \qquad \psi_x(0,t)=0, \qquad \psi_x(l,t)=0, \quad (2a\text{–}d)$$
$$[(F-\mu N)\sec\phi-M_4 a_x(l,t)\sec^2\phi]-KGA[v_x(l,t)-\psi(l,t)]\tan\phi$$
$$-EA[u_x(l,t)+\tfrac{1}{2}v_x^2(l,t)](1+v_x(l,t)\tan\phi)=0. \quad (2e)$$

Equations (1a, b) describe the rigid-body motions of the crank and the connecting rod, respectively, while equations (1c, d, e) describe the flexural vibrations of the connecting rod which is modelled by Timoshenko beam theory. It is seen that the rigid-body motion and the flexural vibrations are coupled. The non-linear partial differential equations (1c, d, e) include the second order spatial derivatives of all the variables u, v and ψ. The five boundary conditions equations (2a, b, c, d, e) and one constraint condition equation (A4) are satisfied to solve the equations (1c, d, e). Boundary condition equation (2d) states that there is zero moment at revoluting joint B, while equation (2e) describes the dynamic behaviour of the slider in the X-direction.

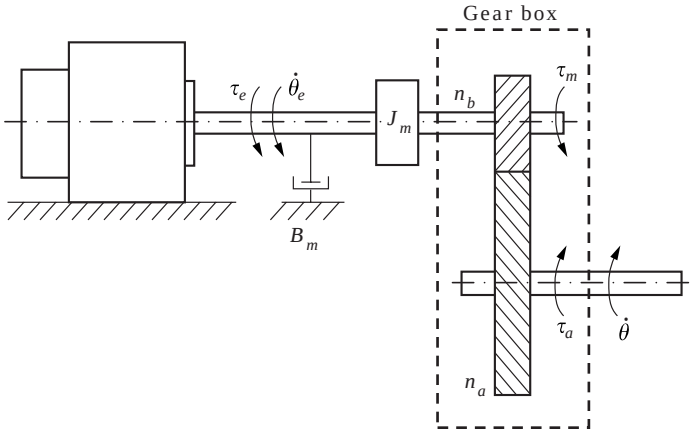

Figure 3. Schematic of the motor-gear-mechanism.

2.2. VARIABLE TRANSFORMATION

Defining the following dimensionless variables and parameters as

$$U = \frac{u}{l}, \qquad V = \frac{v}{l}, \qquad \xi = \frac{x}{l}, \qquad R = \frac{r}{l}, \qquad \tau = \omega_T t,$$

$$\omega_T^2 = \frac{\pi^4 EI}{\rho A l^4}, \qquad \omega_L^2 = \frac{\pi^4 EA}{\rho A l^2}, \qquad S_4 = \frac{M_4}{\rho A l}, \qquad S_2 = \frac{M_2}{\rho A l},$$

$$\zeta^2 = \frac{\omega_T^2}{\omega_L^2}, \qquad \omega_s^2 = \frac{\pi^4 KGA}{\rho A l^2}, \qquad \eta^2 = \frac{\omega_T^2}{\omega_S^2}, \qquad \Lambda = \frac{\lambda}{\rho A l^2 \omega_T^2},$$

$$\varepsilon_1 = \frac{C_x}{\rho A \omega_T}, \qquad \epsilon_2 = \frac{C_y}{\rho A \omega_T}, \qquad \epsilon_3 = \frac{C_\psi}{\rho A \omega_T}, \qquad \bar{F} = \frac{F - \mu N}{\rho A l^2 \omega_T^2},$$

$$I_q^* = \frac{g_r K_t i_q^*}{\rho A l^2 \omega_T^2}, \qquad \bar{J}_m = \frac{g_r^2 J_m}{\rho A l^2}, \qquad \bar{B}_m = \frac{g_r^2 B_m}{\rho A l^2 \omega_T},$$

and substituting into equations (1a–e) and (2a–e) and the constraint condition (A4), we have the dimensionless governing equations

$$\begin{aligned}
\int_0^1 & - R\{R\theta_{\tau\tau} - [U_{\tau\tau} + V\phi_{\tau\tau} + 2V_\tau \phi_\tau - (\xi + U)\phi_\tau^2] \sin(\theta + \phi) \\
& + [V_{\tau\tau} - (\xi + U)\phi_{\tau\tau} - 2U_\tau \phi_\tau - \phi_\tau^2 V] \cos(\theta + \phi)\} \, \mathrm{d}\xi \\
& - S_4 R\{R\theta_{\tau\tau} - [U_{\tau\tau} + V\phi_{\tau\tau} + 2V_\tau \phi_\tau - (1 + U)\phi_\tau^2] \sin(\theta + \phi) \\
& + [V_{\tau\tau} - (1 + U)\phi_{\tau\tau} - 2U_\tau \phi_\tau - \phi_\tau^2 \mathrm{V}] \cos(\theta + \phi)\} + \Lambda R \cos\theta \\
& - \tfrac{1}{3} S_2 R^2 \theta_{\tau\tau} - \bar{J}_m \theta_{\tau\tau} - \bar{B}_m \theta_\tau = -I_q^*,
\end{aligned} \tag{3a}$$

$$\begin{aligned}
\int_0^1 & \{[R\theta_{\tau\tau} \sin(\theta + \phi) + R\theta_\tau^2 \cos(\theta + \phi) - U_{\tau\tau} - 2V_\tau \phi_\tau - V\phi_{\tau\tau}]V \\
& + (\xi + U)[R\theta_{\tau\tau} \cos(\theta + \phi) - R\theta_\tau^2 \sin(\theta + \phi) + V_{\tau\tau} - 2U_\tau \phi_\tau - (\xi + U)\phi_{\tau\tau}] \\
& + \zeta^2(\phi_{\tau\tau} - \Psi_{\tau\tau} + \phi_{\tau\tau} \Psi^2 + 2\phi_\tau \Psi_\tau \Psi)\} \, \mathrm{d}\xi \\
& + S_4 \{[R\theta_{\tau\tau} \sin(\theta + \phi) + R\theta_\tau^2 \cos(\theta + \phi) - U_{\tau\tau} - 2V_\tau \phi_\tau - V\phi_{\tau\tau}]V \\
& + (1 + U)[R\theta_{\tau\tau} \cos(\theta + \phi) - R\theta_\tau^2 \sin(\theta + \phi) + V_{\tau\tau} - 2U_\tau \phi_\tau - (1 + U)\phi_{\tau\tau}]\} \\
& - \Lambda \cos\phi - \left\{\frac{1}{\pi^4 \zeta^2} V_\xi (U_\xi + \tfrac{1}{2} V_\xi^2) + \frac{1}{\pi^4 \eta^2}(V_\xi - \Psi) + S_4 [R\theta_{\tau\tau} \cos(\theta + \phi) \right. \\
& \left. - R\theta_\tau^2 \sin(\theta + \phi) - 2\phi_\tau U_\tau - V\phi_\tau^2 + V_{\tau\tau} - (1 + U)\phi_{\tau\tau}]\right\} U(1, \tau) \sec^2\phi = 0,
\end{aligned} \tag{3b}$$

$$\begin{aligned}
& U_{\tau\tau} + \epsilon_1 U_\tau - R\theta_\tau^2 \cos(\theta + \phi) + 2\phi_\tau V_\tau - (\xi + U)\phi_\tau^2 \\
& \quad - R\theta_{\tau\tau} \sin(\theta + \phi) + V\phi_{\tau\tau} - \frac{1}{\pi^4 \zeta^2}(U_{\xi\xi} + V_\xi V_{\xi\xi}) = 0,
\end{aligned} \tag{3c}$$

$$V_{\tau\tau} + \epsilon_2 V_\tau - R\theta_\tau^2 \sin(\theta+\phi) - 2\phi_\tau U_\tau - \phi_\tau^2 V - (\xi + U)\phi_{\tau\tau} + R\theta_{\tau\tau}\cos(\theta+\phi)$$
$$-\frac{1}{\pi^4\zeta^2}(V_\xi U_{\xi\xi} + \tfrac{3}{2} V_\xi^2 V_{\xi\xi} + U_\xi V_{\xi\xi}) - \frac{1}{\pi^4\eta^2}(V_{\xi\xi} - \Psi_\xi) = 0, \tag{3d}$$

$$\Psi_{\tau\tau} + \frac{\epsilon_3}{\zeta^2}\Psi_\tau + \frac{1}{\pi^4\eta^2\zeta^2}(\Psi - V_\xi) - \phi_\tau^2 \Psi - \frac{1}{\pi^4\zeta^2}\Psi_{\xi\xi} - \phi_{\tau\tau} = 0, \tag{3e}$$

and the boundary conditions

$$U(0,\tau) = 0, \qquad V(0,\tau) = 0, \qquad \Psi_\xi(0,\tau) = 0, \tag{4a–c}$$

$$\Psi_\xi(1,\tau) = 0, \tag{5a}$$

$$\bar{F}\sec\phi - S_4 A_x(1,\tau)\sec^2\phi - \frac{1}{\pi^4\eta^2}[V_\xi(1,\tau) - \Psi(1,\tau)]\tan\phi$$
$$-\frac{1}{\pi^4\zeta^2}[U_\xi(1,\tau) + \tfrac{1}{2} V_\xi^2(1,\tau)](1 + V_\xi(1,\tau)\tan\phi) = 0, \tag{5b}$$

where

$$A_x(1,\tau) = \frac{a_x(1,\tau)}{l\omega_T^2} = -R\theta_{\tau\tau}\sin(\theta+\phi) - R\theta_\tau^2\cos(\theta+\phi)$$
$$+ U_{\tau\tau} + 2V_\tau\phi_\tau + V\phi_{\tau\tau} - (1+U)\phi_\tau^2,$$

and the dimensionless constraint conditions in equations (A4), (A5), (A8) and (A9) are

$$V(1,\tau) = U(1,\tau)\tan\phi, \tag{5c}$$

$$\mathbf{\Phi}(\boldsymbol{\varphi}) = R\sin\theta - \sin\phi = 0, \tag{6a}$$

$$\mathbf{\Phi}_\varphi \boldsymbol{\varphi}_\tau = R\theta_\tau\cos\theta - \phi_\tau\cos\phi = 0, \tag{6b}$$

$$\mathbf{\Phi}_\varphi \boldsymbol{\varphi}_{\tau\tau} = R\theta_\tau^2\sin\theta - \phi_\tau^2\sin\phi \equiv \gamma. \tag{6c}$$

In order to apply the Galerkin method, it is necessary to simplify and change the boundary conditions (5b) and (5c) from non-homogeneous to homogeneous by using the following variable transformation [9] as

$$U(1,\tau) = h(\tau), \tag{7a}$$

$$U(\xi,\tau) = \tilde{U}(\xi,\tau) + \xi\cdot h(\tau), \tag{7b}$$

$$V(\xi,\tau) = \tilde{V}(\xi,\tau) + \xi\cdot h(\tau)\tan\phi. \tag{7c}$$

The physical interpretation of $h(\tau)$ is the non-dimensional axial deformation of the connecting rod at $\xi = 1$. Substituting equations (7a–c) into equations (3a–e) and using equation (5c), one obtains the following equations of motion

$$\int_0^1 -R\{R\theta_{\tau\tau} - [\tilde{U}_{\tau\tau} + \tilde{V}\phi_{\tau\tau} + 2\phi_\tau\tilde{V}_\tau - \phi_\tau^2\tilde{U} + \xi(h_{\tau\tau} + 2h_\tau\phi_\tau\tan\phi$$
$$+ h(\phi_{\tau\tau}\tan\phi + \phi_\tau^2 + 2\phi_\tau^2\sec^2\phi) - \phi_\tau^2)]\sin(\theta+\phi)$$
$$+ [\tilde{V}_{\tau\tau} - \tilde{U}\phi_{\tau\tau} - 2\phi_\tau\tilde{U}_\tau - \phi_\tau^2\tilde{V} + \xi(h_{\tau\tau}\tan\phi + 2h_\tau\phi_\tau\tan^2\phi$$
$$+ h(\phi_{\tau\tau}\tan^2\phi + \phi_\tau^2\tan\phi(2\sec^2\phi - 1)) - \phi_{\tau\tau})]\cos(\theta+\phi)\}\,\mathrm{d}\xi$$
$$- S_4 R\{R\theta_{\tau\tau} - (\tilde{U}_{\tau\tau} + \tilde{V}\phi_{\tau\tau} + 2\phi_\tau\tilde{V}_\tau - \phi_\tau^2\tilde{U} + (h_{\tau\tau} + 2h_\tau\phi_\tau\tan\phi$$

$$+h(\phi_{\tau\tau}\tan\phi+\phi_\tau^2+2\phi_\tau^2\sec^2\phi)-\phi_\tau^2)]\sin(\theta+\phi)$$
$$+[\tilde V_{\tau\tau}-\tilde U\phi_{\tau\tau}-2\phi_\tau\tilde U_\tau-\phi_\tau^2\tilde V+(h_{\tau\tau}\tan\phi+2h_\tau\phi_\tau\tan^2\phi$$
$$+h(\phi_{\tau\tau}\tan^2\phi+\phi_\tau^2\tan\phi(2\sec^2\phi-1))-\phi_{\tau\tau})]\cos(\theta+\phi)\}$$
$$+\Lambda R\cos\theta-\tfrac{1}{3}S_2R^2\theta_{\tau\tau}-\bar J_m\theta_{\tau\tau}-\bar B_m\theta_\tau=-I_q^*, \tag{8a}$$

$$\int_0^1\{[\xi R((h+1)\cos(\theta+\phi)+h\tan\phi\sin(\theta+\phi))+R(\cos(\theta+\phi)\tilde U$$
$$+\sin(\theta+\phi)\tilde V)]\theta_{\tau\tau}+[\xi^2(h\sec^2\phi-2h-1)+\xi((h\sec^2\phi-2(h+1))\tilde U$$
$$-2h\tan\phi\tilde V)-\tilde U^2-\tilde V^2+\zeta^2\Psi^2+\zeta^2]\phi_{\tau\tau}-(\tilde V+\xi h\tan\phi)\tilde U_{\tau\tau}$$
$$+(\tilde U+\xi(1+h))\tilde V_{\tau\tau}+[\xi^2\tan\phi+\xi(\tan\phi\tilde U-\tilde V)]h_{\tau\tau}-\zeta^2\Psi_{\tau\tau}$$
$$+[2\xi h\sec^2\phi(\xi\tan\phi+\tan\phi\tilde U-\tilde V)]\phi_\tau^2+[\xi R(h\tan\phi\cos(\theta+\phi)$$
$$-(h+1)\sin(\theta+\phi))+R\cos(\theta+\phi)\tilde V-R\sin(\theta+\phi)\tilde U]\theta_\tau^2+2[\xi^2h_\tau\tan^2\phi$$
$$-\xi((h+1)\tilde U_\tau-h_\tau\tan^2\phi\tilde U+\tan\phi(\tilde V_\tau h+\tilde V h_\tau))+\zeta^2\phi_\tau\Psi-\tilde U\tilde U_\tau-\tilde V\tilde V_\tau]\phi_\tau\}\,dx$$
$$+S_4\{[R(h+1)\cos(\theta+\phi)+h\tan\phi\sin(\theta+\phi))+R(\cos(\theta+\phi)\tilde U$$
$$+\sin(\theta+\phi)\tilde V)]\theta_{\tau\tau}+[(h\sec^2\phi-2h-1)+(h\sec^2\phi-2(h+1))\tilde U$$
$$-2h\tan\phi\tilde V-\tilde U^2-\tilde V^2]\phi_{\tau\tau}-(\tilde V+h\tan\phi)\tilde U_{\tau\tau}+(\tilde U+(1+h))\tilde V_{\tau\tau}$$
$$+[\tan\phi+(\tan\phi\tilde U-\tilde V)]h_{\tau\tau}+[2h\sec^2\phi(\tan\phi+\tan\phi\tilde U-\tilde V)]\phi_\tau^2$$
$$+[R(h\tan\phi\cos(\theta+\phi)-(h+1)\sin(\theta+\phi))+R\cos(\theta+\phi)\tilde V$$
$$-R\sin(\theta+\phi)\tilde U]\theta_\tau^2+2[h_\tau\tan^2\phi-((h+1)\tilde U_\tau-h_\tau\tan^2\phi\tilde U+\tan\phi(\tilde V_\tau h+\tilde V h_\tau))$$
$$-\tilde U\tilde U_\tau-\tilde V\tilde V_\tau]\phi_\tau\}-\{S_4R\cos(\theta+\phi)\theta_{\tau\tau}+S_4[(h\tan^2\phi-1)-\tilde U]\phi_{\tau\tau}$$
$$+S_4\tilde V_{\tau\tau}+S_4\tan\phi h_{\tau\tau}+2S_4(h_\tau\tan^2\phi-\tilde U_\tau)\phi_\tau-S_4R\sin(\theta+\phi)\theta_\tau^2$$
$$+S_4[h\tan\phi(2\sec^2\phi-1)-\tilde V]\phi_\tau^2+\frac{1}{\pi^4\eta^2}(h\tan\phi-\Psi+\tilde V_\xi)$$
$$+\frac{1}{\pi^4\zeta^2}[(h+\tfrac{3}{2}h^2\tan^2\phi)\tilde V_\xi+h^2\tan\phi(\tfrac{1}{2}h\tan^2\phi+1)+\tilde V_\xi(\tilde U_\xi+\tfrac{1}{2}\tilde V_\xi^2)$$
$$+h\tan\phi(\tilde U_\xi+\tfrac{3}{2}\tilde V_\xi^2)]\}h\sec^2\phi-\Lambda\cos\phi=0, \tag{8b}$$

$$\tilde U_{\tau\tau}+\epsilon_1\tilde U_\tau+2\phi_\tau\tilde V_\tau-\phi_\tau^2\tilde U+\phi_{\tau\tau}\tilde V-\frac{1}{\pi^4\zeta^2}(\tilde U_{\xi\xi}+\tilde V_\xi\tilde V_{\xi\xi}+h\tan\phi\tilde V_{\xi\xi})$$
$$+\xi\{h_\tau[\epsilon_1+2\phi_\tau\tan\phi]-h[\phi_\tau^2(1-2\sec^2\phi)+\phi_{\tau\tau}\tan\phi]+h_{\tau\tau}-\phi_\tau^2\}$$
$$-R\theta_\tau^2\cos(\theta+\phi)-R\theta_{\tau\tau}\sin(\theta+\phi)=0, \tag{8c}$$

$$\tilde V_{\tau\tau}+\epsilon_2\tilde V_\tau-2\phi_\tau\tilde U_\tau-\phi_\tau^2\tilde V-\phi_{\tau\tau}\tilde U-\frac{1}{\pi^4\eta^2}(\tilde V_{\xi\xi}-\Psi_\xi)$$
$$-\frac{1}{\pi^4\zeta^2}[\tilde V_\xi\tilde U_{\xi\xi}+h\tan\phi\tilde U_{\xi\xi}+\tfrac{3}{2}(\tilde V_\xi^2+2h\tan\phi\tilde V_\xi+h^2\tan^2\phi)\tilde V_{\xi\xi}$$
$$+\tilde U_\xi\tilde V_{\xi\xi}+h\tilde V_{\xi\xi}]+\xi\{h_{\tau\tau}\tan\phi+h_\tau[\epsilon_2\tan\phi+2\phi_\tau\tan^2\phi]$$
$$+h[\epsilon_2\phi_\tau\sec^2\phi-\phi_\tau^2\tan\phi(1-2\sec^2\phi)+\phi_{\tau\tau}\tan^2\phi)-\phi_{\tau\tau}\}$$
$$-R\theta_\tau^2\sin(\theta+\phi)+R\theta_{\tau\tau}\cos(\theta+\phi)=0, \tag{8d}$$

$$\Psi_{\tau\tau} + \frac{\epsilon_3}{\zeta^2}\Psi_\tau + \frac{1}{\pi^4\eta^2\zeta^2}(\Psi - \tilde{V}_\xi) - \phi_\tau^2\,\Psi - \frac{1}{\pi^4\zeta^2}\Psi_{\xi\xi} \tag{8e}$$

and the boundary conditions are

$$\tilde{U}(0,\tau) = \tilde{V}(0,\tau) = \Psi_\xi(0,\tau) = 0, \tag{9a–c}$$

$$\tilde{U}(1,\tau) = \tilde{V}(1,\tau) = \Psi_\xi(1,\tau) = 0, \tag{10a–c}$$

and (5b) becomes

$$\begin{aligned} h_{\tau\tau} + 2\phi_\tau h_\tau \tan\phi + \frac{1}{\pi^4\eta^2}\frac{1}{S_4}\cos^2\phi\tan\phi[\tilde{V}_\xi(1,\tau) - \Psi(1,\tau)] + h\{(2\sec^2\phi - 1)\phi_\tau^2 \\ + \phi_{\tau\tau}\tan\phi + \frac{1}{\pi^4\eta^2}\frac{1}{S_4}\sin^2\phi + \frac{1}{\pi^4\zeta^2}\frac{1}{S_4}\cos^2\phi[1 + 2\tilde{V}_\xi(1,\tau)\tan\phi \\ + \tfrac{3}{2}\tilde{V}_\xi^2(1,\tau)\tan^2\phi + \tilde{U}_\xi(1,\tau)\tan^2\phi]\} + \frac{1}{\pi^4\zeta^2}\frac{1}{S_4}\cos^2\phi\{\tfrac{1}{2}h^3\tan^4\phi \\ + \tfrac{3}{2}h^2\tan^2\phi[1 + \tilde{V}_\xi(1,\tau)\tan\phi] + [\tilde{U}_\xi(1,\tau) + \tfrac{1}{2}\tilde{V}_\xi^2(1,\tau)][1 + \tilde{V}_\xi(1,\tau)\tan\phi)\} \\ - R\theta_{\tau\tau}\sin(\theta+\phi)\cos^2\phi - R\theta_\tau^2\cos(\theta+\phi)\cos^2\phi - \phi_\tau^2 - \frac{1}{S_4}\bar{F}\cos\phi = 0. \end{aligned} \tag{11}$$

After the variable transformations (7a, b, c), the non-homogeneous boundary conditions (5b, c) are changed to homogeneous boundary conditions (10a, b, c) and one additional equation (11), which describes the axial deformation of the connecting rod at $\xi = 1$.

2.3. GALERKIN METHOD

Satisfying the homogeneous boundary conditions equations (9) and (10), the nth mode solutions of $\tilde{U}$, $\tilde{V}$ and Ψ are

$$\tilde{U}(\xi,\tau) = \sum_{n=1}^{\infty} f_n(\tau)\sin(n\pi\xi),$$

$$\tilde{V}(\xi,\tau) = \sum_{n=1}^{\infty} g_n(\tau)\sin(n\pi\xi),$$

$$\Psi(\xi,\tau) = \sum_{n=1}^{\infty} \Psi_n(\tau)\cos(n\pi\xi). \tag{12}$$

Substituting equation (12) into equations (8a–e) and equation (11) and then applying the Galerkin method, one obtains

$$\begin{aligned} [-R^2(S_4+1) - \tfrac{1}{3}S_2R^2 - \bar{J}_m]\ddot{\theta} + \left[\left(\frac{R}{\sqrt{2}}\sum_{m=1}^{\infty} a_m g_m + R(S_4+\tfrac{1}{2})h\tan\phi\right)\sin(\theta+\phi)\right. \\ \left. + \left(-\frac{R}{\sqrt{2}}\sum_{m=1}^{\infty} a_m f_m - R(S_4+\tfrac{1}{2})(h\tan^2\phi - 1)\right)\cos(\theta+\phi)\right]\ddot{\phi} \\ + \frac{R}{\sqrt{2}}\sum_{m=1}^{\infty} a_m\sin(\theta+\phi)\ddot{f}_m + \frac{R}{\sqrt{2}}\sum_{m=1}^{\infty}\cos(\theta+\phi)\ddot{g}_m \end{aligned}$$

$$+[R(S_4+\tfrac{1}{2})(\sin(\theta+\phi)+\tan\phi\cos(\theta+\phi))]\ddot{h}-\bar{B}_m\ddot{\theta}$$

$$+\Bigg[\sqrt{2}R\sum_{m=1}^{\infty}a_m\dot{g}_m\dot{\phi}-\frac{R}{\sqrt{2}}\sum_{m=1}^{\infty}a_m f_m\dot{\phi}^2+R(2\dot{h}\dot{\phi}\tan\phi+(h-1)\dot{\phi}^2$$

$$+2h\dot{\phi}^2\sec^2\phi)(S_4+\tfrac{1}{2})]\sin(\theta+\phi)+\Bigg[\sqrt{2}\sum_{m=1}^{\infty}a_m\dot{f}_m\dot{\phi}+\frac{1}{\sqrt{2}}\sum_{m=1}^{\infty}a_m g_m\dot{\phi}^2$$

$$-2R\dot{h}\dot{\phi}\tan^2\phi(S_4+\tfrac{1}{2})-R\tan\phi(2\,sec^2\phi-1)(S_4+\tfrac{1}{2})\dot{\phi}^2]\cos(\theta+\phi)$$

$$+\Lambda R\cos\theta=-I_q^*, \tag{13a}$$

$$\Bigg[R((h+1)\cos(\theta+\phi)+h\tan\phi\sin(\theta+\phi))(S_4+\tfrac{1}{2})+\frac{R}{\sqrt{2}}\Bigg(\cos(\theta+\phi)\sum_{m=1}^{\infty}a_m f_m$$

$$+\sin(\theta+\phi)\sum_{m=1}^{\infty}a_m g_m\Bigg)-S_4 Rh\sec^2\phi\cos(\theta+\phi)\Bigg]\ddot{\theta}$$

$$+\Bigg[(h\sec^2\phi-2h-1)(S_4+\tfrac{1}{3})+\frac{1}{\sqrt{2}}\Bigg((h\sec^2\phi-2(h+1))\sum_{m=1}^{\infty}c_m f_m$$

$$-2h\tan\phi\sum_{m=1}^{\infty}c_m g_m\Bigg)-\tfrac{1}{2}\Bigg(\sum_{m=1}^{\infty}f_m^2+\sum_{m=1}^{\infty}g_m^2\Bigg)+\frac{\zeta^2}{2}\sum_{m=1}^{\infty}\Psi_m^2+\zeta^2$$

$$-S_4 h\sec^2\phi\Bigg((h\tan^2\phi-1)-\frac{1}{\sqrt{2}}\sum_{m=1}^{\infty}a_m f_m\Bigg)\Bigg]\ddot{\phi}-\frac{1}{\sqrt{2}}\Bigg(\frac{1}{\sqrt{2}}\sum_{m=1}^{\infty}g_m$$

$$+h\tan\phi\sum_{m=1}^{\infty}c_m\Bigg)\ddot{f}_m+\frac{1}{\sqrt{2}}\Bigg(\frac{1}{\sqrt{2}}\sum_{m=1}^{\infty}f_m+(1+h)\sum_{m=1}^{\infty}c_m-S_4 h\sec^2\phi\sum_{m=1}^{\infty}a_m\Bigg)\ddot{g}_m$$

$$+\Bigg[S_4 h\sec^2\phi\Bigg(\frac{1}{\sqrt{2}}\sum_{m=1}^{\infty}a_m g_m-h\tan\phi(2\sec^2\phi-1)\Bigg)+2h\sec^2\phi\Bigg(\tan\phi(S_4+\tfrac{1}{3})\Bigg)$$

$$+\Bigg[(S_4+\tfrac{1}{3})\tan\phi+\frac{1}{\sqrt{2}}\Bigg(\tan\phi\sum_{m=1}^{\infty}c_m f_m-\sum_{m=1}^{\infty}c_m g_m\Bigg)-S_4 h\sec^2\phi\tan\phi\Bigg]\ddot{h}$$

$$+\frac{1}{\sqrt{2}}\tan\phi\sum_{m=1}^{\infty}c_m f_m-\frac{1}{\sqrt{2}}\sum_{m=1}^{\infty}c_m g_m\Bigg]\dot{\phi}^2+\Bigg[R(h\tan\phi\cos(\theta+\phi)$$

$$-(h+1)\sin(\theta+\phi))(S_4+\tfrac{1}{2})+\frac{R}{\sqrt{2}}\cos(\theta+\phi)\sum_{m=1}^{\infty}a_m g_m$$

$$-\frac{R}{\sqrt{2}}\sin(\theta+\phi)\sum_{m=1}^{\infty}a_m f_m+S_4 Rh\sec^2\phi\sin(\theta+\phi)\Bigg]\dot{\theta}^2+2\Bigg[(S_4+\tfrac{1}{3})\dot{h}\tan^2\phi$$

$$-\left(\frac{1}{\sqrt{2}}(h+1)\sum_{m=1}^{\infty}c_m\dot{f}_m-\frac{1}{\sqrt{2}}\dot{h}\tan^2\phi\sum_{m=1}^{\infty}c_m f_m\right.$$

$$\left.+\tan\phi\left(\frac{1}{\sqrt{2}}h\sum_{m=1}^{\infty}c_m\dot{g}_m+\frac{1}{\sqrt{2}}\dot{h}\sum_{m=1}^{\infty}a_m g_m\right)\right)-\tfrac{1}{2}\sum_{m=1}^{\infty}f_m\dot{f}_m-\tfrac{1}{2}\sum_{m=1}^{\infty}g_m\dot{g}_m$$

$$-\mathrm{S}_4\,h\sec^2\phi\left(\dot{h}\tan^2\phi-\frac{1}{\sqrt{2}}\sum_{m=1}^{\infty}a_m\dot{f}_m\right)\Bigg]\dot{\phi}-\left\{\frac{1}{\pi^4\eta^2}\left(h\tan\phi-\sum_{m=1}^{\infty}(-1)^m\Psi_m\right.\right.$$

$$\left.+\sum_{m=1}^{\infty}(-1)^m(m\pi)g_m\right)+\frac{1}{\pi^4\zeta^2}\Bigg[(h+\tfrac{3}{2}h^2\tan^2\phi)\sum_{m=1}^{\infty}(-1)^m(m\pi)g_m$$

$$+h^2\tan\phi(\tfrac{1}{2}h\tan^2\phi+1)+\left(\sum_{m=1}^{\infty}\sum_{n=1}^{\infty}(-1)^{m+n}(mn\pi^2)f_n+\sum_{m=1}^{\infty}\sum_{n=1}^{\infty}(-1)^m\right.$$

$$\left.\left.\times(mn^2\pi^3)g_n^2\right)g_m+h\tan\phi\left(\sum_{m=1}^{\infty}(-1)^m(m\pi)f_m+\tfrac{3}{2}\sum_{m=1}^{\infty}(m\pi)^2g_m^2\right)\Bigg]\right\}$$

$$\times h\sec^2\phi-\Lambda\cos\phi=0, \tag{13b}$$

$$\ddot{f}_m-\sqrt{2}a_m R\ddot{\theta}\sin(\theta+\phi)+(g_m-\sqrt{2}c_m h\tan\phi)\ddot{\phi}+\sqrt{2}c_m\ddot{h}+\epsilon_1\dot{f}_m+2\dot{\phi}\dot{g}_m$$

$$+\sqrt{2}\mathrm{c}_m\epsilon_1\dot{h}+\left(\frac{1}{\pi^4\zeta^2}(m\pi)^2-\dot{\phi}^2\right)f_m+\frac{1}{\pi^4\zeta^2}\Bigg[-\sum_{n=1}^{\infty}\sum_{i=1}^{\infty}k_{mni}g_i g_n+(m\pi)^2h\tan\phi\,\mathrm{g_m}\Bigg]$$

$$+\sqrt{2}\left\{c_m\left[2\dot{h}\dot{\phi}\tan\phi-h\dot{\phi}^2(1-2\sec^2\phi)-\dot{\phi}^2\right]-Ra_{\mathrm{m}}\dot{\theta}^2\cos(\theta+\phi)\right\}=0, \tag{13c}$$

$$\ddot{g}_m+\sqrt{2}a_m R\ddot{\theta}\cos(\theta+\phi)-[f_m+\sqrt{2}c_m(1-h\tan^2\phi)]\ddot{\phi}+\sqrt{2}c_m\tan\phi\ddot{h}+\epsilon_2\dot{g}_m$$

$$+\sqrt{2}c_m\epsilon_2\tan\phi\dot{h}-2\dot{\phi}\dot{f}_m-\phi^2g_m+\frac{1}{\pi^4\eta^2}((m\pi)^2g_m-(m\pi)\Psi_m)$$

$$-\frac{1}{\pi^4\zeta^2}\Bigg[\frac{1}{\sqrt{2}}\sum_{n=1}^{\infty}\sum_{i=1}^{\infty}k_{mni}f_i g_n-(m\pi)^2h\tan\phi f_m+\tfrac{3}{2}\left(\tfrac{1}{2}\sum_{n=1}^{\infty}\sum_{i=1}^{\infty}\sum_{j=1}^{\infty}l_{mnij}g_j g_i g_n\right.$$

$$\left.+\frac{2}{\sqrt{2}}h\tan\phi\sum_{n=1}^{\infty}\sum_{i=1}^{\infty}k_{mni}g_i g_n-(m\pi)^2h^2\tan^2\phi g_m\right)+\frac{1}{\sqrt{2}}\sum_{n=1}^{\infty}\sum_{i=1}^{\infty}k_{mni}g_i f_n$$

$$\left.-h(m\pi)^2g_m\Bigg]+\sqrt{2}\left\{c_m\left(2\dot{h}\dot{\phi}\tan^2\phi+h(\epsilon_2\dot{\phi}\sec^2\phi-\dot{\phi}^2\tan\phi(1-2\sec^2\phi)\right)\right]\right.$$

$$\left.-Ra_m\dot{\theta}^2\sin(\theta+\phi)\right\}=0, \tag{13d}$$

$$\ddot{\Psi}_m+\frac{\epsilon_3}{\zeta^2}\dot{\Psi}_m+\left(\frac{1}{\pi^4\eta^2\zeta^2}-\dot{\phi}^2+\frac{1}{\pi^4\zeta^2}(m\pi)^2\right)\Psi_m-\frac{1}{\pi^4\eta^2\zeta^2}(m\pi)g_m=0, \tag{13e}$$

$$\ddot{h} - R\ddot{\theta}\sin(\theta+\phi)\cos^2\phi + h\ddot{\phi}\tan\phi + 2\dot{\phi}\dot{h}\tan\phi + \frac{1}{\pi^4\eta^2}\frac{1}{S_4}\cos^2\phi\tan\phi$$

$$\times\left[\sum_{n=1}^{\infty}(n\pi)(-1)^n g_n - \sum_{n=1}^{\infty}(-1)^n\Psi_n\right] + h\Bigg\{(2\sec^2\phi - 1)\dot{\phi}^2 + \frac{1}{\pi^4\eta^2}\frac{1}{S_4}\sin^2\phi$$

$$+\frac{1}{\pi^4\zeta^2}\frac{1}{S_4}\cos^2\phi\Bigg[1 + 2\sum_{n=1}^{\infty}(n\pi)(-1)^n g_n\tan\phi$$

$$+\tfrac{3}{2}\sum_{n=1}^{\infty}\sum_{i=1}^{\infty}(i\pi)(n\pi)(-1)^{n+i}g_i\,g_n\tan^2\phi + \sum_{n=1}^{\infty}(n\pi)(-1)^n f_n\tan^2\phi\Bigg]\Bigg\}$$

$$+\frac{1}{\pi^4\zeta^2}\frac{1}{S_4}\cos^2\phi\{\tfrac{1}{2}h^3\tan^4\phi + \tfrac{3}{2}h^2\tan^2\phi\Bigg[1 + \sum_{n=1}^{\infty}(n\pi)(-1)^n g_n\tan\phi\Bigg]$$

$$+\Bigg[\sum_{n=1}^{\infty}(n\pi)(-1)^n f_n + \tfrac{1}{2}\sum_{n=1}^{\infty}\sum_{i=1}^{\infty}(i\pi)(n\pi)(-1)^{n+i}g_i\,g_n\Bigg]\Bigg[1+\sum_{n=1}^{\infty}(n\pi)(-1)^n g_n\tan\phi\Bigg]\Bigg\}$$

$$- R\dot{\theta}^2\cos(\theta+\phi)\cos^2\phi - \dot{\phi}^2 - \frac{1}{S_4}\bar{F}\cos\phi = 0, \tag{13f}$$

where $(\dot{})$ and $()'$ represent derivatives with respect to the dimensionless time τ and space ξ, respectively. For details of $a_m, b_m, \ldots, l_{mnij}$, see Appendix B.

The Runge–Kutta numerical method will be used to integrate the above ordinary differential equations for the transient solutions of ϕ, θ, h, f_m, g_m and Ψ_m. By substituting the solutions into equation (12) and using equations (7b, c), the transverse and longitudinal displacements, $U(\frac{1}{2},\tau)$ and $V(\frac{1}{2},\tau)$, of the midpoint of the connecting rod are obtained respectively.

Then, equations (13a–f) can be rewritten as the following non-linear coupled set of ordinary differential equations

$$\mathbf{M}(\boldsymbol{\beta})\ddot{\boldsymbol{\beta}} + \mathbf{N}(\boldsymbol{\beta},\dot{\boldsymbol{\beta}}) + \boldsymbol{\Phi}_\beta^T\Lambda = \mathbf{B}\mathbf{U}, \tag{14}$$

where

$$\boldsymbol{\beta} = [\phi \quad \theta \quad h \quad \mathbf{f} \quad \mathbf{g} \quad \boldsymbol{\Psi}]^T,$$

and $\mathbf{f} = [f_1\ f_2\cdots f_m]$, $\mathbf{g} = [g_1\ g_2\cdots g_m]$, $\boldsymbol{\Psi} = [\Psi_1\ \Psi_2\cdots\Psi_m]$. The elements of $\mathbf{M}$, $\mathbf{N}$, $\boldsymbol{\Phi}_\beta$, $\mathbf{B}$ and $\mathbf{U}$ are given in Appendix C.

The constraint position (6a), velocity (6b) and acceleration (6c) must be held at any time. By using equations (6c) and (14), the equation in the matrix form is

$$\begin{bmatrix}\mathbf{M} & \boldsymbol{\Phi}_\beta^T\\ \boldsymbol{\Phi}_\beta & \mathbf{0}\end{bmatrix}\begin{bmatrix}\ddot{\boldsymbol{\beta}}\\ \Lambda\end{bmatrix} = \begin{bmatrix}\mathbf{B}\mathbf{U} - \mathbf{N}(\boldsymbol{\beta},\dot{\boldsymbol{\beta}})\\ \gamma\end{bmatrix}. \tag{15}$$

This is a system of differential-algebraic equations and the matrices element can be found in Appendix C.

2.4. REDUCED SYSTEM OF DIFFERENTIAL EQUATIONS OF MOTION

The differential-algebraic equations of mechanism motion derived above are summarized in the matrix form of equation (15) and the constraint equation (6a). An implicit method will be employed to solve the differential-algebraic equations of the system.

Equations (15) and (6a) may be reordered and partitioned, according to the decomposition of $\boldsymbol{\beta} = [\phi\ \ \theta\ \ h\ \ \mathbf{f}\ \ \mathbf{g}\ \ \boldsymbol{\Psi}]^T$. If the constraints are independent, the matrix $\boldsymbol{\Phi}_\beta$ has full row rank, and there is always at least one non-singular submatrix $\boldsymbol{\Phi}_\beta$ of rank 2 [20]. Gauss–Jordan reduction of the matrix $\boldsymbol{\Phi}_\beta$ with double pivoting defines a partitioning of $\boldsymbol{\beta} = [\mathbf{p}^T\ \ \mathbf{q}^T]^T$, $\mathbf{p} = [\phi]^T$, $\mathbf{q} = [\theta\ \ h\ \ \mathbf{f}\ \ \mathbf{g}\ \ \boldsymbol{\Psi}]^T$ such that $\boldsymbol{\Phi}_p$ is the submatrix of $\boldsymbol{\Phi}_p$ whose columns correspond to elements $\mathbf{p}$ of $\boldsymbol{\beta}$, and $\boldsymbol{\Phi}_q$ is the submatrix of $\boldsymbol{\Phi}_\beta$ whose columns correspond to element $\mathbf{q}$ of $\boldsymbol{\beta}$. The elements of the vectors $\mathbf{p}$ and $\mathbf{q}$, and matrices $\boldsymbol{\Phi}_p$ and $\boldsymbol{\Phi}_q$ are detailed in Appendix D. Thus, equations (15) and (A7) can be rewritten as:

$$\mathbf{M}^{pp}\ddot{\mathbf{p}} + \mathbf{M}^{pq}\ddot{\mathbf{q}} + \boldsymbol{\Phi}_p^T \Lambda = \mathbf{B}^p\mathbf{U} - \mathbf{N}^p,$$

$$\mathbf{M}^{qp}\ddot{\mathbf{p}} + \mathbf{M}^{qq}\ddot{\mathbf{q}} + \boldsymbol{\Phi}_q^T \Lambda = \mathbf{B}^q\mathbf{U} - \mathbf{N}^q,$$

$$\boldsymbol{\Phi}_p\ \ddot{\mathbf{p}} + \boldsymbol{\Phi}_q\ \ddot{\mathbf{q}} = \gamma. \tag{16}$$

Eliminating Λ and $\ddot{\mathbf{p}}$ in the above equations yields

$$\hat{\mathbf{M}}(\mathbf{q})\ddot{\mathbf{q}} + \hat{\mathbf{N}}(\mathbf{q}, \dot{\mathbf{q}}) = \hat{\mathbf{Q}}\mathbf{U}, \tag{17}$$

where

$$\hat{\mathbf{M}} = \mathbf{M}^{qq} - \mathbf{M}^{qp}\boldsymbol{\Phi}_p^{-1}\ \boldsymbol{\Phi}_q - \boldsymbol{\Phi}_q^T\ (\boldsymbol{\Phi}_p^{-1})^T[\mathbf{M}^{pq} - \mathbf{M}^{pp}\boldsymbol{\Phi}_p^{-1}\ \boldsymbol{\Phi}_q],$$

$$\hat{\mathbf{N}} = [\mathbf{N}^q - \boldsymbol{\Phi}_q^T\ (\boldsymbol{\Phi}_p^{-1})^T\mathbf{N}^p] + [\mathbf{M}^{qp}\ \boldsymbol{\Phi}_p^{-1} - \boldsymbol{\Phi}_q^T\ (\boldsymbol{\Phi}_p^{-1})^T\mathbf{M}^{pp}\boldsymbol{\Phi}_p^{-1}]\gamma,$$

$$\hat{\mathbf{Q}} = \mathbf{B}^q - \boldsymbol{\Phi}_q^T\ (\boldsymbol{\Phi}_p^{-1})^T\mathbf{B}^p, \qquad \mathbf{U} = [I_q^*].$$

The result is a set of differential equation with only one independent generalized co-ordinate $\mathbf{q}$. The equation is an initial value problem and can be integrated by using the fourth order Runge–Kutta method.

2.5. STATE VARIABLE REPRESENTATION

Let $\mathbf{X} = [\mathbf{q}, \dot{\mathbf{q}}]^T$ be the state variable vector. Then one can rewrite equation (17) in terms of $\mathbf{X}$ as

$$\dot{\mathbf{X}} = \hat{\mathbf{a}}(\mathbf{X}) + \hat{\mathbf{b}}\mathbf{U}(\tau), \tag{18}$$

where

$$\hat{\mathbf{a}}(\mathbf{X}) = \begin{bmatrix} \dot{\mathbf{q}} \\ -\hat{\mathbf{M}}^{-1}\hat{\mathbf{N}} \end{bmatrix}, \qquad \hat{\mathbf{b}} = \begin{bmatrix} \mathbf{0} \\ \hat{\mathbf{M}}^{-1}\hat{\mathbf{Q}} \end{bmatrix}, \qquad \mathbf{U}(\tau) = [I_q^*].$$

3. DESIGN OF THE VSC CONTROLLER

The variable structure system is a special class of non-linear systems characterized by a discontinuous control action which changes the system structure on the state reaching the switching surface. The major merit of these systems is their insensitivity to parameter variations and external disturbances. In this section, the first object is to design the reaching law VSC via the design of switching functions, the next step is to design the reaching mode and the overall control law which give a desired system dynamics in the reaching mode. The main requirement in the design is that the controller should satisfy the reaching condition, which guarantees the existence of the sliding mode on the switching surface.

3.1. SWITCHING SURFACE SCHEME

In switching surface design, it is essential to use the error signal and its derivatives to form the co-ordinates and the switching surface. When the state variables slide on the switching surface and to the origin, the system error goes to zero and the desired target state is reached.

In this paper, only one input is needed for the motor–mechanism coupled system. Rewriting equation (18) as

$$\ddot{\mathbf{q}} = \mathbf{a}(\mathbf{q}, \dot{\mathbf{q}}) + \mathbf{b}(\mathbf{q})\mathbf{U}(\tau), \tag{19}$$

where $\mathbf{a}(\mathbf{q}, \dot{\mathbf{q}}) = -\hat{\mathbf{M}}^{-1}\hat{\mathbf{N}}$, $\mathbf{b}(\mathbf{q}) = \hat{\mathbf{M}}^{-1}\hat{\mathbf{Q}}$ and $\mathbf{U}(\tau)$ is the control current input I_q^*.

To control the speed vector $\dot{\mathbf{q}}$, many more sophisticated schemes will be necessary. Unlike conventional VSC, the integral variable structure control (IVSC) applied in the speed controller is suitable for the first order system without any information on the acceleration. Furthermore, if one wishes to track the trajectories required for the specified motor revolution, then the tracking controller is designed by the desired motion. The two cases will demonstrate the good performance of the reaching law VSC system. The design procedure can be divided into two subcases as follows.

3.1.1. *Speed controller design*

Let the speed error vector be

$$\mathbf{e} = \dot{\mathbf{q}} - \dot{\mathbf{q}}_d, \tag{20}$$

where the desired speed vector $\dot{\mathbf{q}}_d$ is a constant vector. The resultant error state equation is

$$\dot{\mathbf{e}} = \ddot{\mathbf{q}} - \ddot{\mathbf{q}}_d = \mathbf{a}(\mathbf{q}, \dot{\mathbf{q}}) + \mathbf{b}(\mathbf{q})U - \ddot{\mathbf{q}}_d. \tag{21}$$

Since there is one control input, a single switching surface $S(\mathbf{e})$ will be constructed for the speed control system. By using a scalar function with an integration of the speed error vector $\mathbf{e}$, one has the switching surface [21]

$$S(\mathbf{e}) = \mathbf{C}_1\,\mathbf{e} + \mathbf{C}_2 \int_0^\tau \mathbf{e}(\gamma)\,\mathrm{d}\gamma. \tag{22}$$

It is noted that for the one control input in the first order system (21), only one switching surface (22) is needed. Figure 4 shows the block diagram of the constant speed controller applied to a flexible slider–crank mechanism driven by a PM synchronous servo motor. The controller is called the integral variable structure control (IVSC). Substituting equation (21) into the time derivative of $S(\mathbf{e})$, one obtains

$$\dot{S} = \mathbf{C}_1\,\dot{\mathbf{e}} + \mathbf{C}_2\,\mathbf{e} = \mathbf{C}_1\,[\mathbf{a}(\mathbf{q}, \dot{\mathbf{q}}) + \mathbf{b}(\mathbf{q})\mathbf{U} - \ddot{\mathbf{q}}_d] + \mathbf{C}_2\,\mathbf{e}. \tag{23}$$

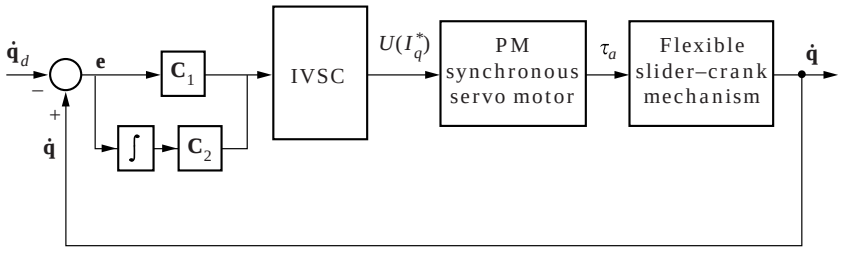

Figure 4. Block diagram of the constant speed controller applied to a flexible slider–crank mechanism driven by a PM synchronous servo motor with IVSC.

3.1.2. *Tracking controller design*

The tracking error vector of the motor revolution is

$$\tilde{\mathbf{e}} = \mathbf{X} - \mathbf{X}_d = \begin{bmatrix} \tilde{\mathbf{e}}_i \\ \dot{\tilde{\mathbf{e}}}_i \end{bmatrix} = \begin{bmatrix} \mathbf{q} - \mathbf{q}_d \\ \dot{\mathbf{q}} - \dot{\mathbf{q}}_d \end{bmatrix}, \tag{24}$$

where $\mathbf{X}_d = [\mathbf{q}_d, \dot{\mathbf{q}}_d]^T$, and the first and second derivatives of $\tilde{\mathbf{e}}_i$ are defined as the following

$$\dot{\tilde{\mathbf{e}}}_i = \tilde{\mathbf{e}}_j = \dot{\mathbf{q}} - \dot{\mathbf{q}}_d, \tag{25a}$$

$$\ddot{\tilde{\mathbf{e}}}_i = \dot{\tilde{\mathbf{e}}}_j = \ddot{\mathbf{q}} - \ddot{\mathbf{q}}_d = \mathbf{a}(\mathbf{q}, \dot{\mathbf{q}}) + \mathbf{b}(\mathbf{q})\mathbf{U} - \ddot{\mathbf{q}}_d. \tag{25b}$$

A single switching function $S(\mathbf{e})$ for the second order system equation (25) is

$$S(\tilde{\mathbf{e}}) = \mathbf{C}\tilde{\mathbf{e}} = [\mathbf{C}_i \quad \mathbf{C}_j] \begin{bmatrix} \tilde{\mathbf{e}}_i \\ \tilde{\mathbf{e}}_j \end{bmatrix} = \mathbf{C}_i\, \tilde{\mathbf{e}}_i + \mathbf{C}_j\, \tilde{\mathbf{e}}_j, \tag{26}$$

Substituting equations (25a, b) into the time derivative of $S(\tilde{\mathbf{e}})$, one can obtain

$$\dot{S} = \mathbf{C}_i\, \dot{\tilde{\mathbf{e}}}_i + \mathbf{C}_j\, \dot{\tilde{\mathbf{e}}}_j = \mathbf{C}_i\, \tilde{\mathbf{e}}_j + \mathbf{C}_j\, [\mathbf{a}(\mathbf{q}, \dot{\mathbf{q}}) + \mathbf{b}(\mathbf{q})\mathbf{U} - \ddot{\mathbf{q}}_d]. \tag{27}$$

The position control can also be obtained in the tracking control as if the desired position, speed and acceleration are time-independent in the control process. Figure 5 shows the block diagram of the tracking controller.

3.2. REACHING MODE DESIGN AND CONTROL LAW

The treatment given here is to define the reaching law with proportional plus constant power rates:

$$\dot{S} = -PS - Q|S|^k \operatorname{sgn}(S), \qquad 0 < \kappa < 1, \tag{28}$$

where P and Q are positive constant coefficients. This reaching law decreases the reaching time and increases the reaching speed when the state is far away from the switching surface [22, 23].

Thus, by using the above reaching law (28), the state is forced to approach the switching surface faster and the chattering is also suppressed. It is noted that the selection of equation (28) guarantees the convergence of the trajectories to the switching surface. Sliding will occur along the hyperplane $S = 0$ as long as the necessary hitting condition [24]:

$$S\dot{S} < 0 \tag{29}$$

exists. By substituting equations (22) and (23) into equation (29) for the speed controller and substituting equations (26) and (27) into equation (29) for the tracking controller, the

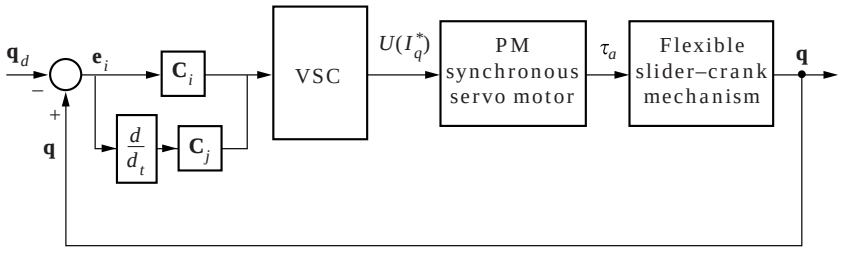

Figure 5. Block diagram of the tracking controller applied to a flexible slider–crank mechanism driven by a PM synchronous servo motor with VSC.

convergence condition (29) is always satisfied regardless of the signs of equations (22) and (26). Thus, one can obtain the control laws as follows.

3.2.1. *Speed controller design*

The single input for the speed controller design is

$$\mathbf{U} = -(\mathbf{C}_1\,\mathbf{b}(\mathbf{q}))^{-1}[\mathbf{C}_2\,\mathbf{e} + \mathbf{C}_1\,(\mathbf{a}(\mathbf{q},\dot{\mathbf{q}}) - \ddot{\mathbf{q}}_d) + PS + Q|S|^{\kappa}\,\mathrm{sgn}\,(S)]. \tag{30}$$

3.2.2. *Tracking controller design*

The single input for the tracking controller design is

$$\mathbf{U} = -(\mathbf{C}_j\,\mathbf{b}(\mathbf{q}))^{-1}[\mathbf{C}_i\,\tilde{\mathbf{e}}_j + \mathbf{C}_j\,(\mathbf{a}(\mathbf{q},\dot{\mathbf{q}}) - \ddot{\mathbf{q}}_d) + PS + Q|S|^{\kappa}\,\mathrm{sgn}\,(S)]. \tag{31}$$

In the conventional VSC, there exists the undesirable steady state error owing to the non-ideal sliding mode. The proposed IVSC scheme for speed control gives the additional advantage of improving the steady state performance.

In order to reduce the chattering, the sgn (S) in the discontinuous control laws (30) and (31) is replaced by a saturation function inside the boundary layer [25]. The saturation function is

$$\mathrm{sat}\,(S) = \begin{cases} S/\Delta, & |S| \leqslant \Delta, \\ \mathrm{sgn}\,(S), & |S| > \Delta, \end{cases} \tag{32}$$

where Δ is a boundary layer width.

4. NUMERICAL RESULTS AND DISCUSSIONS

In the numerical simulations, parameters of the slider–crank mechanism are chosen as: $l = 0{\cdot}1524$ m; $d = 0{\cdot}00635$ m; $R = 0{\cdot}3$, $M_2 = 0{\cdot}2$ kg, $M_4 = 0{\cdot}03781$ kg, $\rho = 0{\cdot}007834\ \mathrm{N}\cdot\mathrm{s}^2/\mathrm{m}^4$, $E = 2{\cdot}068 \times 10^{11}\ \mathrm{N/m}^2$, $G = 80 \times 10^9\ \mathrm{N/m}^2$, $K = 0{\cdot}886$, $I = 7{\cdot}981 \times 10^{-11}\ \mathrm{m}^4$, $\epsilon_1 = 0{\cdot}2$, $\epsilon_2 = 0{\cdot}2$, $\epsilon_3 = 0{\cdot}001$, $g_r = 1$, $\kappa = 0{\cdot}3$ and $\Delta = 0{\cdot}5$. The parameters of the motor are: $K_t = 0{\cdot}6732\ \mathrm{N}\cdot\mathrm{m/A}$, $J_m = 1{\cdot}32 \times 10^{-3}\ \mathrm{N}\cdot\mathrm{m}\cdot\mathrm{s}^2$, $B_m = 5{\cdot}78 \times 10^{-3}\ \mathrm{N}\cdot\mathrm{m}\cdot\mathrm{s/rad}$.

By using the Runge–Kutta method, equation (18) is solved for the motor-mechanism coupled system. Numerical results are divided into two parts: (1) dynamic analysis and (2) vibration control. Each part includes a constant angular velocity and a trapezoidal angular velocity of the crank rotation.

4.1. DYNAMIC ANALYSIS

4.1.1. *Constant angular velocity*

The crank rotates with a constant angular velocity $\dot{\theta}(\tau) = 0{\cdot}2$. The initial conditions are $\mathbf{p}(0) = \dot{\mathbf{p}}(0) = \mathbf{q}(0) = \mathbf{0}$, and $\dot{\mathbf{q}}(0) = [0{\cdot}2\ \ 0\ \ \mathbf{0}\ \ \mathbf{0}\ \ \mathbf{0}]^T$. The results in Figures 6(a)–(f) show the transient amplitudes of the first (solid line), the second (dash line) and the third (dash-dotted line) modes. It is seen that the responses of the higher modes are only small percentages of those of the first mode. The transverse amplitude g in Figure 6(b) is about 500 times of the longitudinal amplitude f in Figure 6(a). The transient rotary angles ψ due to bending are shown in Figure 6(c). The longitudinal amplitudes at the end point of the connecting rod are shown in Figure 6(d). Figures 6(e)–(f) represent the transverse responses at $\xi = 1/2$ and $\xi = 1$, respectively. In Figures 6(a) and (d), the system oscillates violently first and then approaches a stable state because of the introduction of damping terms ϵ_1, ϵ_2 and ϵ_3.

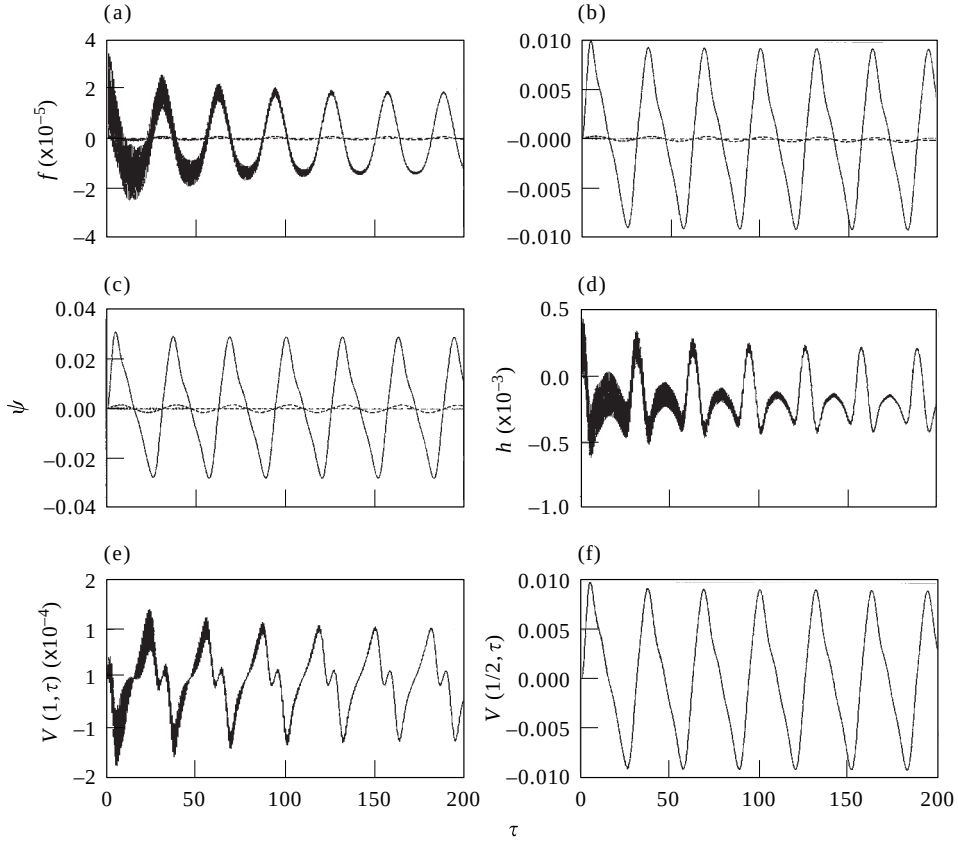

Figure 6. Transient displacements of the first three modes of the flexible connecting rod for a constant angular velocity $\dot{\theta} = 0{\cdot}2$: (a) longitudinal amplitudes f; (b) transverse amplitudes g; (c) rotary angles ψ; (d) axial deformation $h(\tau)$ at the end point B; (e) transverse deformation $V(1, \tau)$; (f) transverse deformation $V(1/2, \tau)$. (First mode ——, second mode ----, third mode –·–·.)

4.1.2. *Trapezoidal angular velocity*

In many applications, a motor is used to drive the flexible systems. Usually, the velocity input is a trapezoidal shape. As show in Figure 7(b), the prescribed angular velocity is $\dot{\theta}_d(\tau)$ is

$$\dot{\theta}_d(\tau) = \begin{cases} \dfrac{0{\cdot}2\tau}{\tau_1} & 0 < \tau \leqslant \tau_1, \\ 0{\cdot}2 & \tau_1 < \tau \leqslant \tau_2, \\ \dfrac{0{\cdot}2(\tau - \tau_3)}{(\tau_2 - \tau_3)} & \tau_2 < \tau \leqslant \tau_3, \\ 0 & \tau_3 < \tau. \end{cases}$$

The initial conditions are $\mathbf{p}(0) = \dot{\mathbf{p}}(0) = \mathbf{q}(0) = \dot{\mathbf{q}}(0) = \mathbf{0}$. Figures 7(a)–(h) compare the transient amplitudes between the results of Case 1: $\tau_1 = 40$, $\tau_2 = 110$, $\tau_3 = 150$ (solid line) and Case 2: $\tau_1 = 50$, $\tau_2 = 100$, $\tau_3 = 150$ (dash line). Because Case 1 has a faster speed-up and faster speed-down in the transient processes ($0 \leqslant \tau \leqslant 40$ and $110 \leqslant \tau \leqslant 150$), it is observed that the amplitudes of Case 1 are larger than those in Case 2. In the constant angular velocity

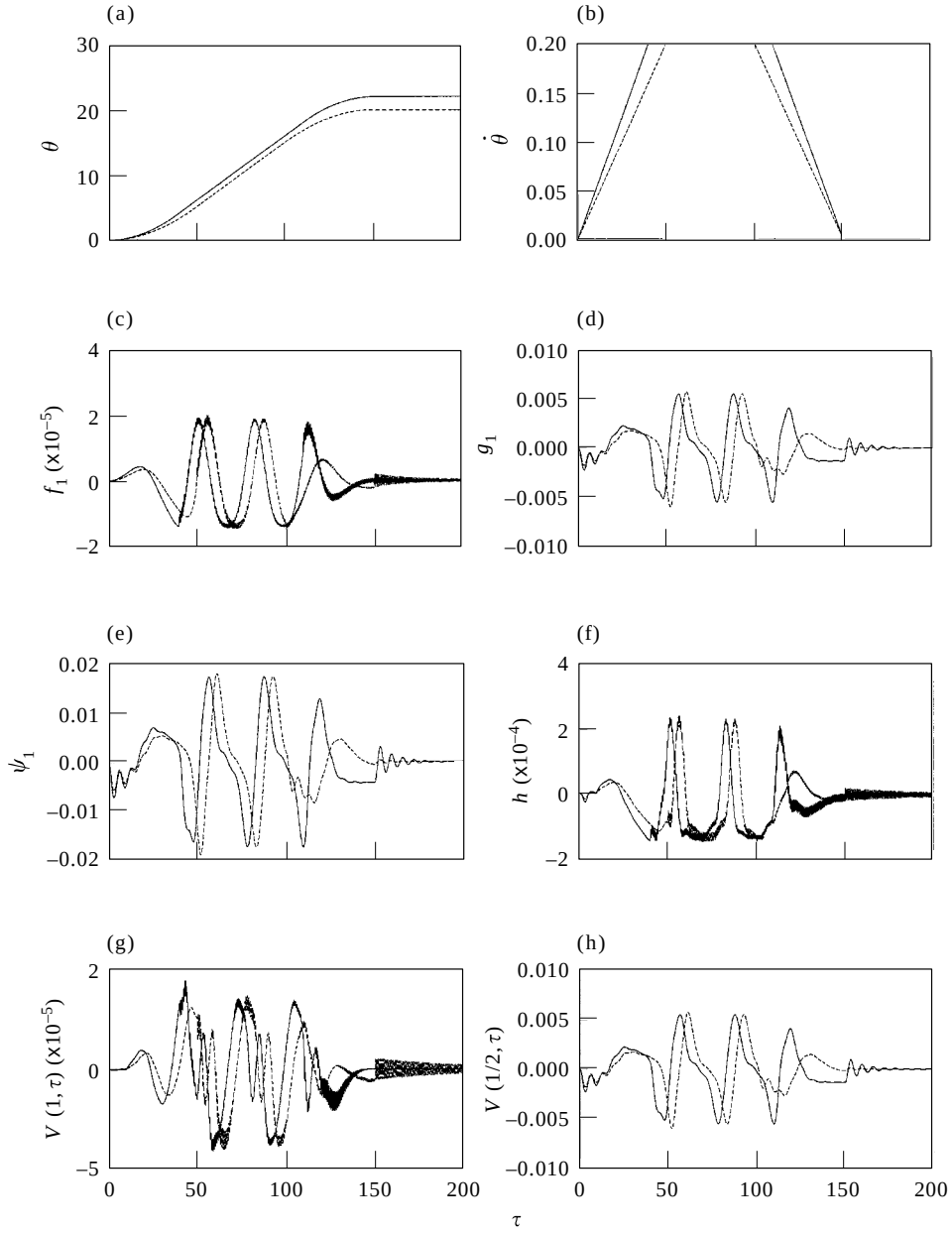

Figure 7. Tip transient displacements of the flexible rod for a trapezoidal angular velocity: (a) desired angle θ; (b) desired angular velocity $\dot{\theta}$, (c) longitudinal amplitude f_1; (d) transverse amplitude g_1; (e) rotary angle ψ_1; (f) axial deformation $h(\tau)$ at the end point B; (g) transverse deformation $V(1, \tau)$; (h) transverse deformation $V(1/2, \tau)$. (Case 1 ——, Case 2 ----.)

process the amplitudes of both cases are equal but with a time ($\tau = 10$) shift. After $\tau > 150$, the motion-induced vibrations occur, and both amplitudes gradually decrease to zero. This is because part of the energy of the rigid-body motion goes into the flexible deformations of the links and is dissipated by the viscous damping.

4.2. VIBRATION CONTROL

Yeung and Chen [26–28] used the pole placement method to obtain good dynamic responses of flexible robot arms. However, their method has only been applied to linear systems associated with the constant symmetry inertia matrices. In this paper, the non-linearity and asymmetry inertia matrices are included in the system, and the traditional trial-and-error method will be applied to choose the gains of the control laws

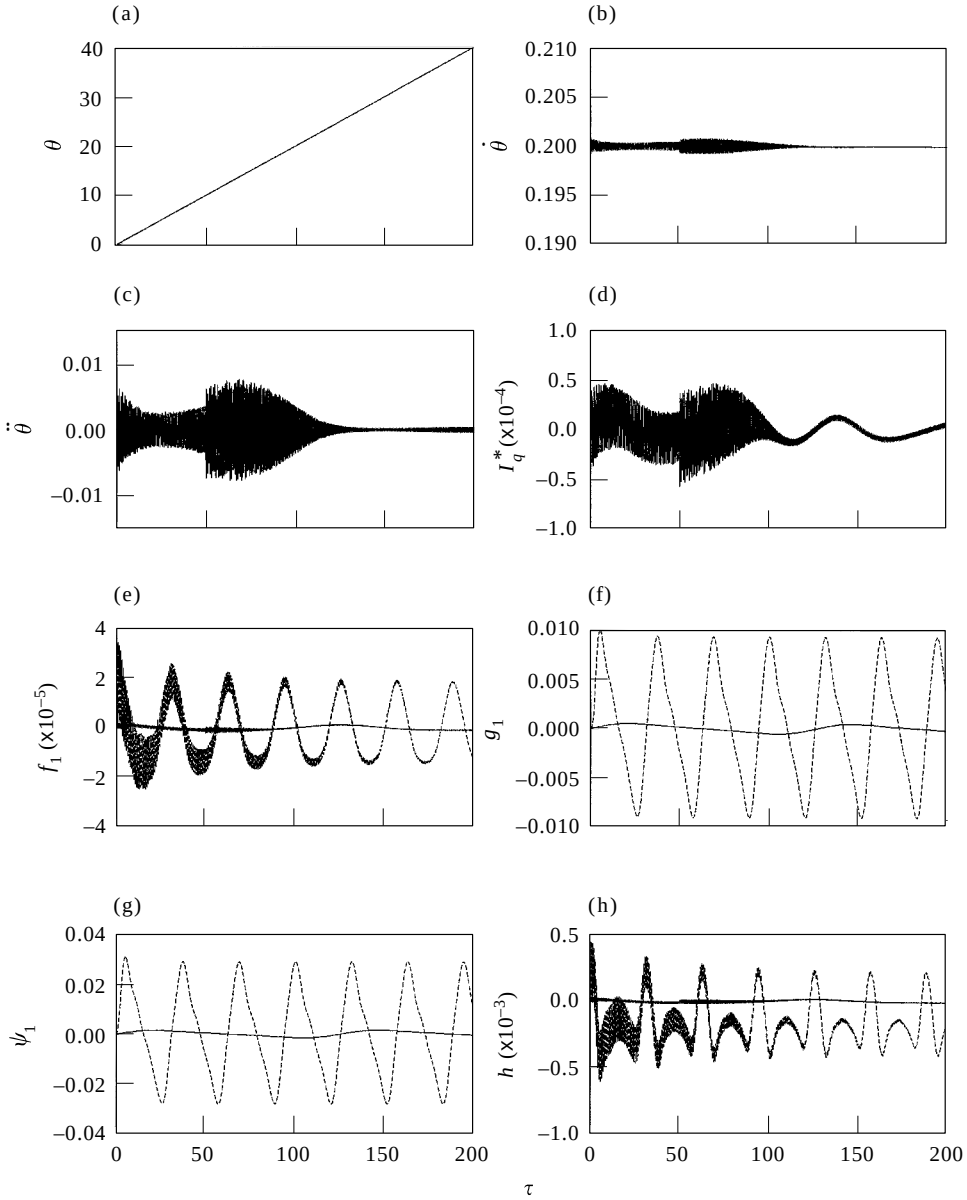

Figure 8. Constant angular velocity controlled by the proposed VSC law: (a) crank angle θ; (b) crank angular velocity $\dot{\theta}$; (c) crank angular acceleration $\ddot{\theta}$; (e) longitudinal amplitude f_1; (f) transverse amplitude g_1; (g) rotary angle ψ_1; (h) axial deformation $h(\tau)$ at the end point B. (Controlled ——, uncontrolled ----.)

in the following sections. Since the responses of the higher modes are small enough to be negligible, the first-mode amplitude of the connecting rod will be considered only in the vibration control.

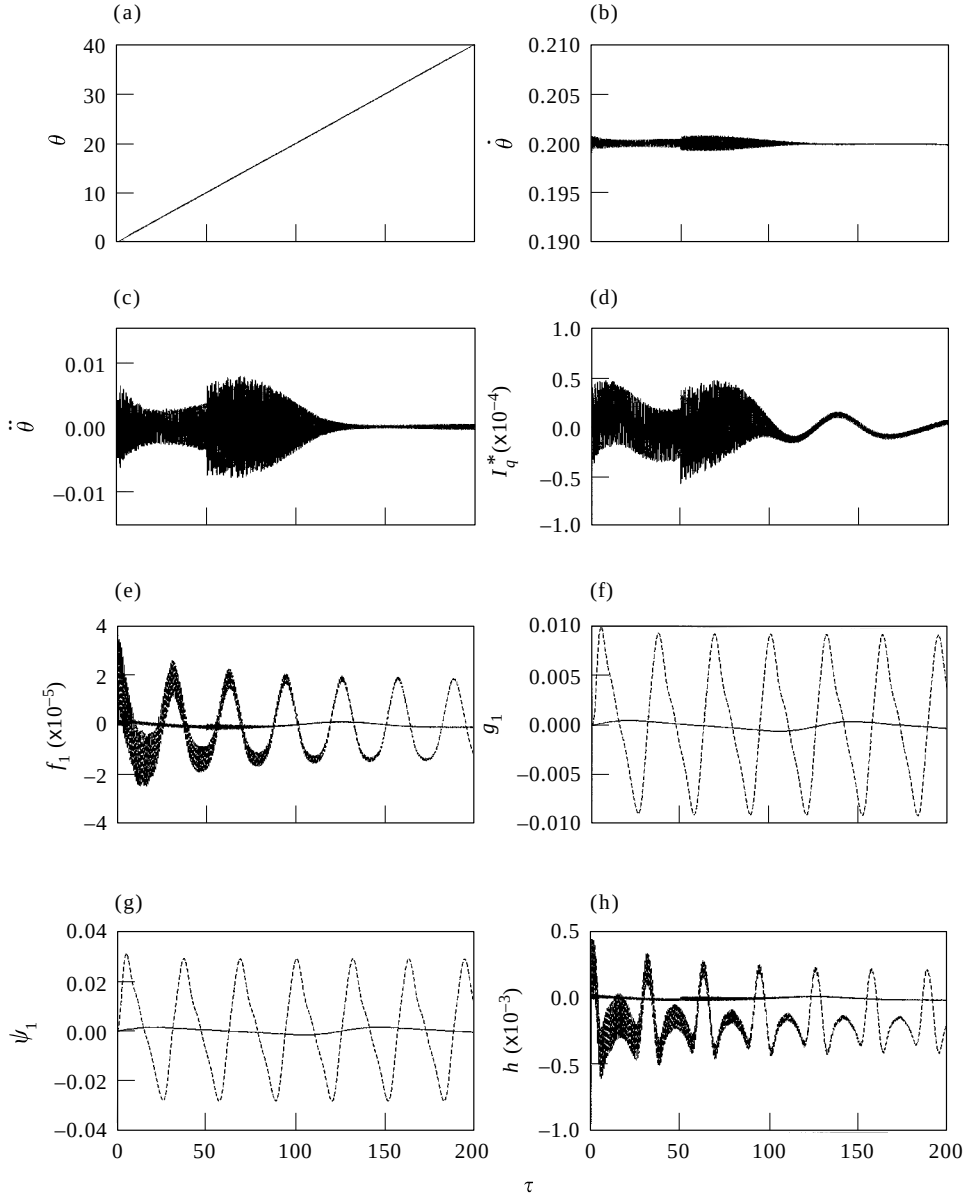

Figure 9. Constant angular velocity controlled by the proposed VSC law with external disturbance $F = 49$ N during $50 \leqslant \tau \leqslant 200$: (a) crank angle θ; (b) crank angular velocity $\dot{\theta}$; (c) crank angular acceleration $\ddot{\theta}$; (e) longitudinal amplitude f_1; (f) transverse amplitude g_1; (g) rotary angle ψ_1; (h) axial deformation $h(\tau)$ at the end point B. (Controlled ——, uncontrolled ----.)

4.2.1. *Constant angular velocity control*

By trial and error, the gain matrices for the switching function are chosen as

$$\mathbf{C}_i = [0{\cdot}06 \quad 0{\cdot}03 \quad 0{\cdot}02 \quad 0{\cdot}008 \quad 0{\cdot}005],$$

$$\mathbf{C}_j = [0{\cdot}5 \quad 0{\cdot}65 \quad 0{\cdot}8 \quad -0{\cdot}05 \quad -0{\cdot}02],$$

$P = 0{\cdot}003$ and $Q = 0{\cdot}0002$. The transient responses are shown in Figures 8(a)–(h). Figures 8(a)–(c) show the crank angle, angular velocity and angular acceleration,

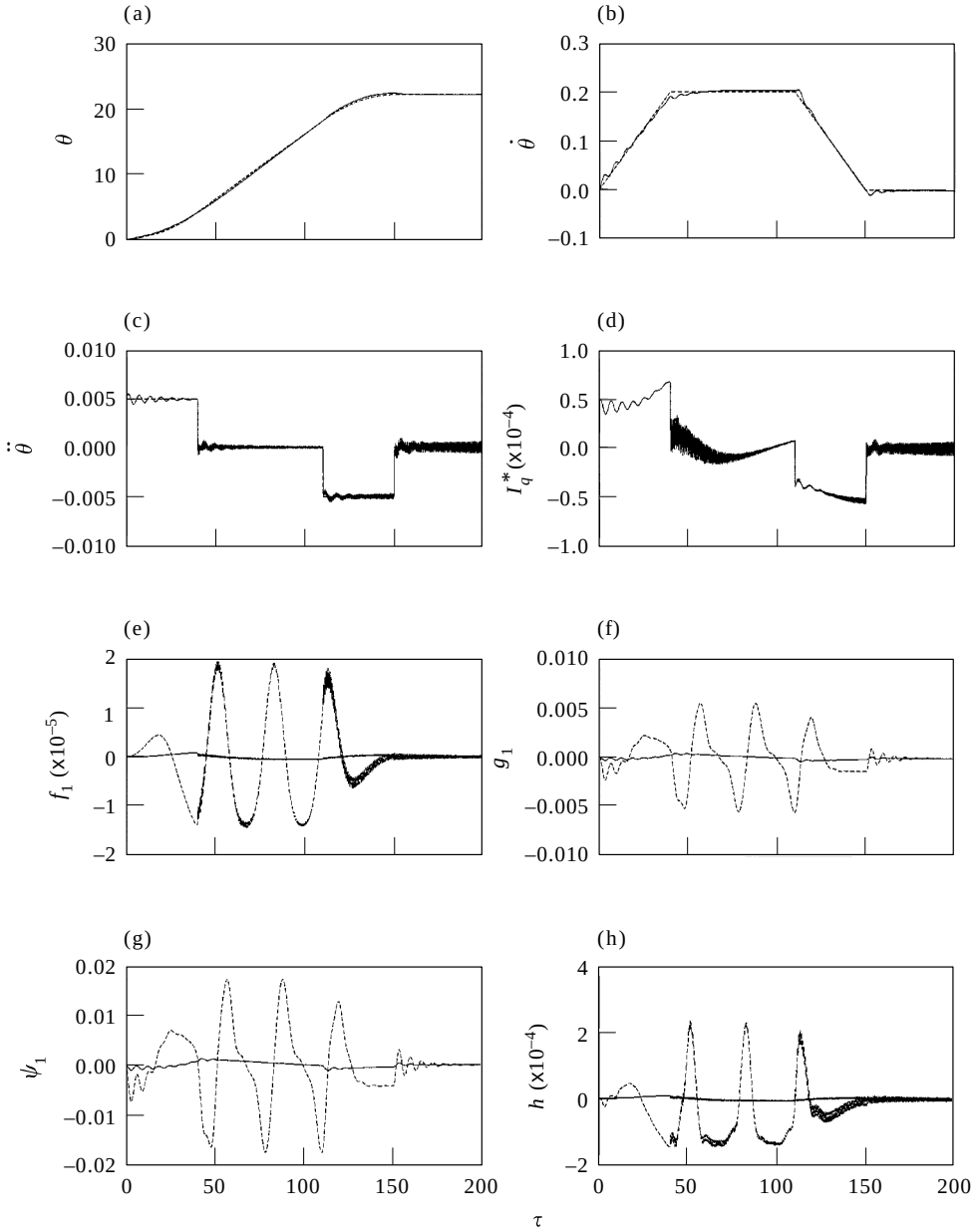

Figure 10. Controlled tip deflection for a prescribed trapezoidal angular velocity; (a) crank angle θ, (b) crank angular velocity $\dot{\theta}$; (c) crank angular acceleration $\ddot{\theta}$; (e) longitudinal amplitude f_1; (f) transverse amplitude g_1; (g) rotary angle ψ_1; (h) axial deformation $h(\tau)$ at the end point B. (Controlled ——, uncontrolled ----.)

respectively. Figure 8(d) shows the dimensionless current input. It is seen that the angular velocity and acceleration, and the dimensionless current input have the observable chattering at the start process. In Figures 8(e)–(h), it is shown that the proposed VSC law decreases the longitudinal and transverse amplitudes, rotary angle and axial deformation at end point (solid lines). The responses for speed control with an external disturbance ($F = 49$ N) applied during $50 \leqslant \tau \leqslant 200$ are shown in Figures 9(a)–(h). In Figure 9(b) the

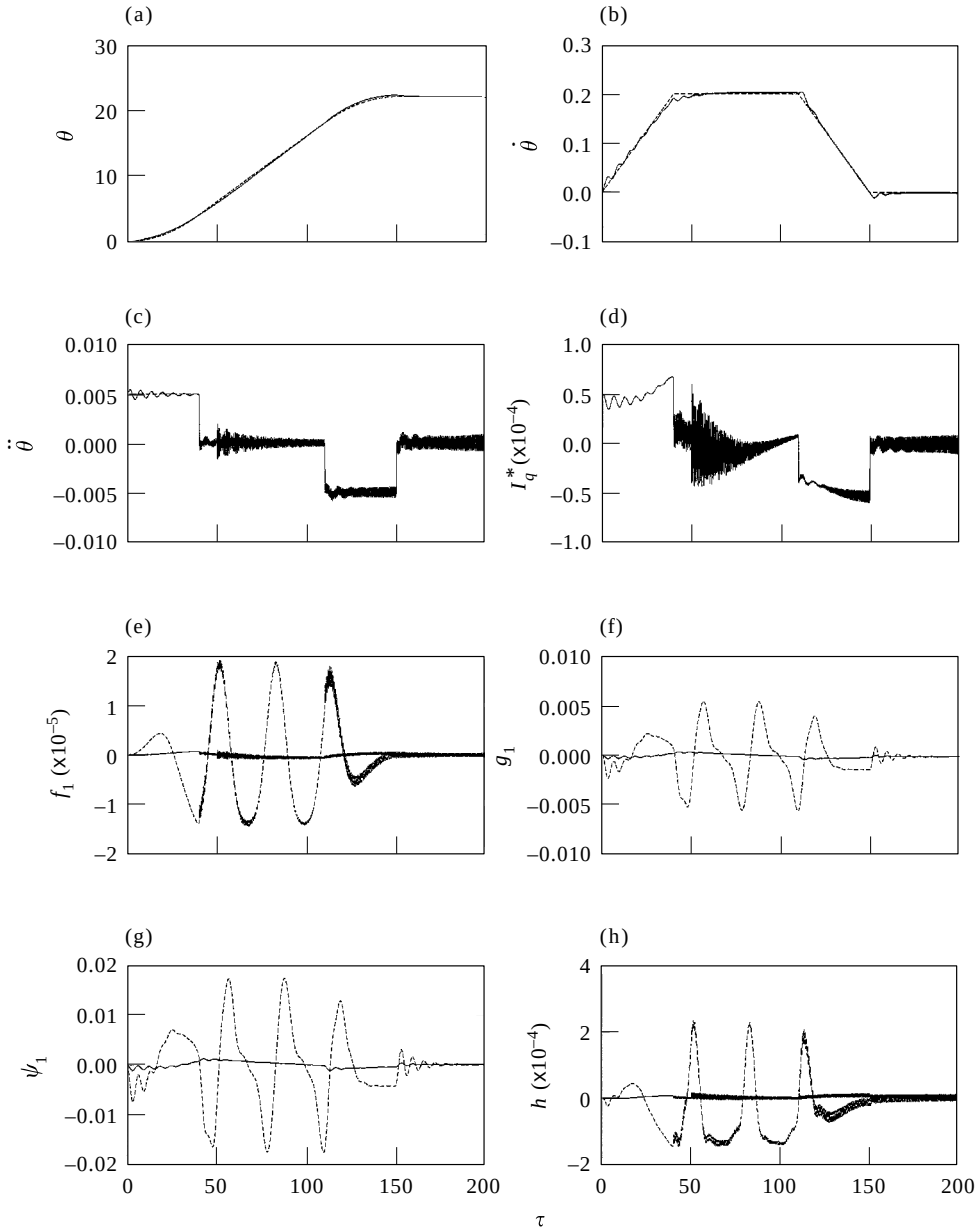

Figure 11. Controlled tip deflection for a prescribed trapezoidal angular velocity with external disturbance $F = 49$ N during $50 \leqslant \tau \leqslant 200$: (a) crank angle θ; (b) crank angular velocity $\dot{\theta}$; (c) crank angular acceleration $\ddot{\theta}$; (e) longitudinal amplitude f_1; (f) transverse amplitude g_1; (g) rotary angle ψ_1; (h) axial deformation $h(\tau)$ at the end point B. (Controlled ——, uncontrolled ----.)

angular velocity response is completely robust with perfect rejection of disturbance, but the larger amplitudes of I_q^* during $50 \leqslant \tau \leqslant 200$ as shown in Figure 9(d) are diminished at sacrifice of the disturbance rejection. The transient behaviours of the longitudinal amplitudes f_1, transverse amplitudes g_1 and rotary angles ψ_1 in Figures 9(e)–(g) are almost the same as Figures 8(e)–(g).

4.2.2. *Trapezoidal angular velocity control*

The desired trapezoidal trajectory is assumed to be the same as Case 1 in section 4.1.2. By choosing the proper gain matrices $\mathbf{C}_i$, $\mathbf{C}_j$ and constant coefficients P and Q, the flexible deflections will be bounded in an allowance range. The gain matrices for the switching surface are

$$\mathbf{C}_i = [5 \quad 6 \quad 12 \quad 0{\cdot}08 \quad 0{\cdot}05], \qquad \mathbf{C}_j = [50 \quad 10 \quad 30 \quad 0{\cdot}75 \quad 0{\cdot}35],$$

$P = 0{\cdot}05$ and $Q = 0{\cdot}0025$, which are chosen by trial and error. The transient responses (dash line, without control) for the desired trapezoidal angular velocity are shown in Figures 10(a)–(h). In order to suppress the deflections in Figures 10(e)–(h), the crank angle, velocity and acceleration have slight changes with respect to the desired trapezoidal trajectories. The current input in Figure 10(d) also has chattering. The suppressed amplitudes are shown by solid lines in Figures 10(e)–(h). Figures 11(a)–(h) show the robustness with respect to the external disturbances. The external force ($F = 49$ N) is considered as a disturbance during $50 \leqslant \tau \leqslant 200$. In order to reject the disturbance, the control input in Figure 11(d) is larger than that in Figure 10(d). In Figure 11(d), it is obvious that the higher control input provides the higher torque to the mechanism during impacting disturbance. The deflections in Figures 11(e)–(h) only have slight changes as compared to those in Figures 10(e)–(h). This means that the proposed controller–motor–mechanism coupled system is robust to the external disturbance.

5. CONCLUSIONS

The dynamic analysis and vibration control of a flexible slider–crank mechanism driven by a PM synchronous servo motor have been studied in this paper. Hamilton's principle is employed to derive the governing equations of the whole system including the slider–crank mechanism and the servo motor. The boundary condition of the connecting rod moving with the slider is the time-dependent boundary support, but not the purely simple support. When the rigid crank rotates, the motion-induced vibrations occur at the flexible connecting rod. To suppress the vibrations, we have successfully designed a new method called reaching law variable structure control (VSC) method.

The significant contributions of the flexible slider–crank mechanism system are summarized as follows. (1) The controller, motor and slider–crank mechanism coupled system have been derived completely with the crank operating with a non-constant speed. (2) A transformation method is successfully used to treat the non-homogenous boundary condition. (3) The design procedure of vibration control can also be applied to any other mechanism with more than one flexible connecting rod. (4) The design procedure of VSC is simple. Numerical results have shown that the proposed VSC not only eliminates deflections of the flexible connecting rod, but also keeps good tracking performances. (5) Robust control performances of the controller–motor–mechanism coupled system are obtained by the proposed controllers with respect to the external disturbance.

ACKNOWLEDGMENTS

The authors are greatly indebted to the support of the National Science Council R.O.C. through contact no. NSC 87–2212-E-033–016 and Chung Yuan Christian University through contact no. CY 85-RG-004.

REFERENCES

1. P. W. Jasinski, H. C. Lee and G. N. Sandor 1971 *Transactions of the American Society of Mechanical Engineers*, *Journal Engineering for Industry* **5**, 636–644. Vibrations of elastic connecting rod of a high-speed slider–crank mechanism.
2. Z. G. Zhu and Y. Chen 1983 *Transactions of the American Society of Mechanical Engineers*, *Journal of Mechanism*, *Transmissions and Automation in Design* **105**, 637–640. The stability of the motion of a connecting rod.
3. M. Badlani and W. Kleinhenz 1979 *Transactions of the American Society of Mechanical Engineers*, *Journal of Mechanical Design* **101**, 149–153. Dynamic stability of elastic mechanism.
4. B. V. Viscomi and R. S. Arye 1971 *Transactions of the American Society of Mechanical Engineers*, *Journal Engineering for Industry* **93**, 251–262. Nonlinear dynamic response of elastic slider–crank mechanism.
5. S. Y. Lu, I. Haque and A. Lakshmikumaran 1995 *Journal of Sound and Vibration* **182**, 3–22. An investigation of the dynamic stability of a slider–crank mechanism with link and drive train flexibility.
6. S. C. Chu and K. C. Pan 1975 *Transactions of the American Society of Mechanical Engineers*, *Journal of Engineering for Industry* **May**, 542–550. Dynamic response of a high-speed slider–crank mechanism with an elastic connecting rod.
7. J. P. Sadler and G. N. Sandor 1973 *Transactions of the American Society of Mechanical Engineers*, *Journal of Engineering for Industry* **May**, 549–557. A lumped parameter approach to vibration and stress analysis of elastic linkages.
8. J. Lieh 1994 *Mechanism and Machine Theory* **29**, 139–147. Dynamic modeling of a slider–crank mechanism with coupler and joint flexibility.
9. R. F. Fung 1996 *Transactions of the American Society of Mechanical Engineers*, *Journal of Vibration and Acoustics* **118**, 687–689. Dynamic analysis of the flexible connecting rod of a slider–crank mechanism.
10. H. T. Wu and N. K. Mani 1994 *Transactions of the American Society of Mechanical Engineers*, *Journal of Mechanical Design* **116**, 437–444. Modeling of flexible bodies for multibody dynamic systems using Ritz vectors.
11. T. S. Liu and J. C. Lin 1993 *Transactions of the American Society of Mechanical Engineers*, *Journal of Vibration and Acoustics* **115**, 468–476. Forced vibration of flexible body systems: a dynamic stiffness method.
12. B. Fallahi, S. Lai and C. Venkat 1995 *Transactions of the American Society of Mechanical Engineers*, *Journal of Dynamic Systems*, *Measurement*, *and Control* **117**, 329–335. A finite element formulation of a flexible slider crank mechanism using local coordinates.
13. K. M. Hsiao and R. T. Yang 1996 *Journal of Sound and Vibration* **190**, 177–194. Effect of member initial curvature on a flexible mechanism response.
14. R. F. Fung and H. H. Chen 1997 *Journal of Sound and Vibration* **199**, 237–251. Steady-state response of the flexible connecting rod of a slider–crank mechanism with time-dependent boundary condition.
15. J. Y. S. Luh, M. W. Walker and R. P. Paua 1982 *Transactions of the American Society of Mechanical Engineers*, *Journal of Dynamic System*, *Measurement and Control* **102**, 126–133. Resolved motion force control of robot manipulators.
16. A. Flcola, M. L. Cava and P. Muraca 1992 *IFAC Motion Control for Intelligent Automation Perugia*, *Italy* **October**, 27–29. A simplified strategy to implement sliding mode control of a two-joints robot with a flexible forearm.
17. S. B. Choi, C. C. Cheong and H. C. Shin 1995 *Journal of Sound and Vibration* **179**, 737–748. Sliding mode control of vibration in a single-link flexible arm with parameter variations.
18. B. K. Bose 1988 *Institute of Electrical and Electronic Engineers*, *Transactions on Industry Electronics* **35**, 160–176. Technology trends in microcomputer control of electrical machines.

19. W. LEONNARD 1986 *Automatica* **22**, 1–19. Microcomputer control of high dynamic performance ac drives: a survey.
20. R. A. WEHAGE and E. J. HAUG 1982 *Transactions of the American Society of Mechanical Engineers*, *Journal of Mechanism Design* **104**, 247–255. Generalized coordinate partitioning for dimension reduction in analysis of constrained dynamic systems.
21. S. K. CHUNG, J. H. LEE, J. S. KO and M. J. YOUN 1995 *Institute of Electrical Engineering Proceedings—Electronics Power Application* **142**, 361–370. Robust speed control of brushless direct-drive motor using integral variable structure control.
22. W. GEO and J. C. HUNG 1993 *Institute of Electrical and Electronic Engineers*, *Transactions on Industrial Electronics* **40**, 45–55. Variable structure control of nonlinear systems: a new approach.
23. W. J. WANG and J. L. LEE 1993 *Journal of Control Systems and Technology* **1**, 19–25. Hitting time reduction and chattering attenuation in variable structure systems.
24. U. ITKIS 1976 *Control System of Variable Structure*. New York: Wiley.
25. J. J. SLOTINE and S. S. SASTRY 1983 *International Journal of Control* **38**, 465–492. Tracking control of nonlinear systems using sliding surface with application to robot manipulators.
26. Y. P. CHEN and K. S. YEUNG 1991 *International Journal of Control* **54**, 257–278. Sliding-mode control of multi-link flexible manipulator.
27. K. S. YEUNG and Y. P. CHEN 1989 *International Journal of Control* **49**, 1965–1978. Regulation of a one-link flexible robot arm using sliding mode technique.
28. K. S. YEUNG and Y. P. CHEN 1990 *International Journal of Control* **52**, 101–117. Sliding-mode controller design of a single-link flexible manipulator under gravity.
29. I. G. TADJBAKHSH and C. J. YOUNIS 1986 *Transactions of the American Society of Mechanical Engineers*, *Journal of Mechanism*, *Transmissions and Automation in Design* **108**, 487–496. Dynamic stability of the flexible connecting rod of a slider crank mechanism.
30. N. MOHAN, T. R. UNDELAND and W. P. ROBBINS 1989 *Power Electronics*. New York: Wiley, second edition.

APPENDIX A

The displacement field of the deformed beam is shown in Figure 1. **i**, **j** are the unit vectors of the fixed co-ordinate system (OXY), and $\mathbf{e}_r$, $\mathbf{e}_\theta$ and $\mathbf{e}_i$, $\mathbf{e}_j$ are the unit vectors of the moving co-ordinates with origins at O and A respectively.

The displacement field of the Timoshenko beam is

$$u_1(x, y, t) = u(x, t) - y\psi(x, t), \tag{A1}$$

$$u_2(x, y, t) = v(x, t), \tag{A2}$$

where u and v represent the axial and transverse displacements of any point on the connecting rod, and ψ is the slope of the deflection curve due to bending deformation alone. The position vector of one arbitrary point P on the connecting rod is

$$\begin{aligned}\mathbf{R}(x, y, t) &= r\mathbf{e}_r + (x + u_1)\mathbf{e}_i + (y + u_2)\mathbf{e}_j \\ &= [r\cos\theta + (x + u - y\psi)\cos\phi + (y + v)\sin\phi]\mathbf{i} \\ &\quad + [r\sin\theta - (x + u - y\psi)\sin\phi + (y + v)\cos\phi]\mathbf{j}.\end{aligned}$$

Since the slider moves along the X-axis, the point B, where the connecting rod is pinned to the slider, also moves along the X-axis. Thus, the constraint condition of point B is

$$\begin{aligned}0 &= \mathbf{R}(l, 0, t)\cdot\mathbf{j} \\ &= r\sin\theta - [l + u(l, t)]\sin\phi + v(l, t)\cos\phi,\end{aligned}$$

which means that the displacement is always zero in the Y direction. Substituting the geometric relation

$$r \sin \theta = l \sin \phi, \tag{A3}$$

into the above equation, one has

$$v(l, t) = u(l, t) \tan \phi. \tag{A4}$$

The above displacement relationship at point B can also be obtained from the geometric plot shown in Figure 2.

The holomonic constraint equation is

$$\mathbf{\Phi}(\varphi) = r \sin \theta - l \sin \phi = 0, \tag{A5}$$

where $\boldsymbol{\varphi} = [\theta \ \ \phi]^T$ is the vector of generalized co-ordinates.

The kinematic velocity and acceleration are obtained by taking the first and second derivatives of equation (A5), respectively, as

$$\mathbf{\Phi}_{\varphi} \, \boldsymbol{\varphi}_t = 0, \tag{A6}$$

and

$$\mathbf{\Phi}_{\varphi} \, \boldsymbol{\varphi}_{tt} = -(\mathbf{\Phi}_{\varphi} \, \boldsymbol{\varphi}_t)_{\varphi} \, \boldsymbol{\varphi}_t \equiv \gamma, \tag{A7}$$

where

$$\mathbf{\Phi}_{\varphi} \, \boldsymbol{\varphi}_t = r\theta_t \cos \theta - l\phi_t \cos \phi, \tag{A8}$$

$$\mathbf{\Phi}_{\varphi} \, \boldsymbol{\varphi}_{tt} = r\theta_t^2 \sin \theta - l\phi_t^2 \sin \phi. \tag{A9}$$

It is seen that $u(l, t) = v(l, t) = 0$ for the assumption of a simply-supported end [6, 29] is also included in equation (A4). If the axial displacement $u(x, t)$ is negligible (i.e., only the transverse displacement $v(x, t)$ is considered), the constraint condition at point B becomes $v(l, t) = 0$, and it becomes a simply supported end. In the present work, the axial and transverse displacements are considered simultaneously; $u(l, t)$ and $v(l, t)$ are not independent and related by equation (A4). Taking the variation of equation (A4), we have

$$\delta v(l, t) = \delta u(l, t) \tan \phi + u(l, t) \sec^2 \phi \delta\phi. \tag{A10}$$

Substituting equation (A10) into $\delta\mathbf{R}(x, y, t)$, taking $x = l$ and $y = 0$, one has

$$\delta\mathbf{R}(l, 0, t) = \delta u(l, t)\mathbf{e}_i + \delta v(l, t)\mathbf{e}_j = \delta u(l, t) \sec \phi \mathbf{i}.$$

Differentiating $\mathbf{R}(x, y, t)$ with respect to time, one gets the absolute velocity of the arbitrary point P on the connecting rod as

$$\begin{aligned} \mathbf{R}_t \, (x, y, t) &= r\theta_t \, \mathbf{e}_\theta + (u_t - y\psi_t)\mathbf{e}_i + v_t \, \mathbf{e}_j \\ &\quad - \phi_t \, \mathbf{e}_k \times [(x + u - y\psi)\mathbf{e}_i + (y + v)\mathbf{e}_j] \\ &= [-r\theta_t \sin (\theta + \phi) + u_t - y\psi_t + \phi_t \, (y + v)]\mathbf{e}_i \\ &\quad + [r\theta_t \cos (\theta + \phi) + v_t - \phi_t \, (x + u - y\psi)]\mathbf{e}_j. \end{aligned} \tag{A11}$$

Because the slider moves in the X direction and the component of the acceleration of the connecting rod in the Y direction is zero, the acceleration of point B can be written as

$$\mathbf{R}_{tt} \, (l, 0, t) = a_x \, (l, t) \sec \phi \mathbf{i},$$

where

$$a_x(l, t) = \mathbf{R}_{tt}(l, 0, t) \cdot \mathbf{e}_i$$
$$= -r\theta_{tt} \sin(\theta + \phi) - r\theta_t^2 \cos(\theta + \phi)$$
$$+ u_{tt} + 2v_t \phi_t + v\phi_{tt} - (l + u)\phi_t^2. \tag{A12}$$

The kinetic energy of the connecting rod can be expressed as

$$T_3 = \tfrac{1}{2} \int_V \rho \mathbf{R}_t(x, y, t) \cdot \mathbf{R}_t(x, y, t)\, \mathrm{d}V = \int_0^l T^* \,\mathrm{d}x, \tag{A13}$$

where

$$T^* = \frac{\rho A}{2} \{[-r\theta_t \sin(\theta + \phi) + u_t + v\phi_t]^2 + [r\theta_t \cos(\theta + \phi) + v_t - \phi_t(x + u)]^2\}$$
$$+ \frac{\rho I}{2} [(\phi_t - \psi_t)^2 + \phi_t^2 \psi^2]. \tag{A14}$$

The Lagrangian strains are

$$\epsilon_{xx} = u_x - y\psi_x + \tfrac{1}{2} v_x^2, \tag{A15}$$

$$\epsilon_{yy} = 0, \tag{A16}$$

$$\epsilon_{xy} = \tfrac{1}{2} [-\psi + v_x + (u_x - y\psi_x)(-\psi)] \approx \tfrac{1}{2}(v_x - \psi), \tag{A17}$$

where the higher order terms $u_x \psi$, $y\psi\psi_x$ are neglected in ϵ_{xy}. The strain energy of the connecting rod can be expressed as

$$U_3 = \tfrac{1}{2} \int_V \sigma_{ij} \epsilon_{ij}\, \mathrm{d}V = \int_0^l U^* \,\mathrm{d}x, \tag{A18}$$

where

$$U^* = \tfrac{1}{2} [EA(u_x + \tfrac{1}{2} v_x^2)^2 + KGA(v_x - \psi)^2 + EI\psi_x^2]. \tag{A19}$$

The kinetic energy of the crank with mass M_2 is

$$T_2 = \tfrac{1}{2} (\tfrac{1}{3} M_2 r^2) \theta_t^2 = \tfrac{1}{6} M_2 r^2 \theta_t^2. \tag{A20}$$

The kinetic energy of the slider is

$$T_4 = \tfrac{1}{2} M_4 \mathbf{R}_t(l, 0, t) \cdot \mathbf{R}_t(l, 0, t). \tag{A21}$$

Figure 3 shows a PM synchronous servo motor system including a motor-gear mechanism and the output torque is applied to a flexible slider–crank mechanism. It is noted that g_r is the gear ratio, K_t is the motor torque constant, i_q^* is q-axis current, J_m is the rotor moment of inertia and B_m is the damping factor. The virtual work done by the external force F, and the friction force μN acting on the slider, and the driving torque τ_a applied on the crank [30] is

$$\delta W^A = [(F - \mu N)\mathbf{i} + N\mathbf{j}] \delta \mathbf{R}(l, 0, t) + \tau_a\, \delta\theta$$
$$= (F - \mu N) \delta u(l, 0, t) \sec\phi + g_r (K_t i_q^* - g_r J_m \theta_{tt} - g_r B_m \theta_t) \delta\theta. \tag{A22}$$

The generalized constraint reaction force can be obtained in terms of the Lagrange multiplier as:

$$\mathbf{Q}^C = \mathbf{\Phi}_\varphi^T \lambda,$$

where

$$\mathbf{\Phi}_\varphi = [r\cos\theta - l\cos\phi]. \tag{A23}$$

Thus, the virtual work by all constraint forces is

$$\delta W^C = \delta\boldsymbol{\varphi}^T \mathbf{Q}^C. \tag{A24}$$

By using Hamilton's principle, one can write

$$0 = \int_{t_1}^{t_2} \left\{ \int_0^l \delta L \, \mathrm{d}x + \delta T_2 + \delta T_4 + \delta W^4 + \delta W^C \right\} \mathrm{d}t, \tag{A25}$$

where $L(\theta, \theta_t, \phi, \phi_t, u, u_t, u_x, v, v_t, v_x, \psi, \psi_t, \psi_x) = T^* - U^*$ is the Lagrangian density of the servo motor and the slider–crank mechanism.

The point $(x, y) = (0, 0)$ is the common revoluting joint of the rigid crank and the flexible connecting rod, and the values $u(0, t) = 0$ and $v(0, t) = 0$ are specified, thus one have $\delta u(0, t) = 0$ and $\delta v(0, t) = 0$. The slope angles ψ at the end points $x = 0, l$ of the connecting rod are free, therefore $\delta\psi(0, t) \neq 0$ and $\delta\psi(l, t) \neq 0$.

Substituting equations (A13, A18, A21, A22) into equation (A25), using the constraint condition (A10) at $x = l$ and introducing the damping terms C_x, C_y and C_ψ, which are proportional to the relative velocities u_t, v_t and ψ_t, one obtains the governing equations (1a–e) and the boundary conditions (2a–e).

APPENDIX B

Define

$$Y_m(\xi) = \sqrt{2}\sin(m\pi\xi), \qquad Z_m(\xi) = \sqrt{2}\cos(m\pi\xi),$$
$$Y_n(\xi) = \sqrt{2}\sin(n\pi\xi), \qquad Z_n(\xi) = \sqrt{2}\cos(n\pi\xi),$$

and

$$a_m = \int_0^1 Y_m(\xi)\,\mathrm{d}\xi = \frac{\sqrt{2}}{m\pi}[(-1)^{m+1} + 1],$$

$$b_m = \int_0^1 Z_m(\xi)\,\mathrm{d}\xi = 0,$$

$$c_m = \int_0^1 \xi Y_m(\xi)\,\mathrm{d}\xi = \frac{\sqrt{2}}{m\pi}(-1)^{m+1},$$

$$d_{mn} = \int_0^1 Y_n(\xi) Y_m(\xi)\,\mathrm{d}\xi = \begin{cases} 1, & \text{if } m = n, \\ 0, & \text{if } m \neq n, \end{cases}$$

$$e_{mn} = \int_0^1 Z_n(\xi) Z_m(\xi)\,\mathrm{d}\xi = \begin{cases} 1, & \text{if } m = n, \\ 0, & \text{if } m \neq n, \end{cases}$$

$$f_{mn} = \int_0^1 Y_n'(\xi) Y_m(\xi)\,\mathrm{d}\xi = \begin{cases} 0, & \text{if } m = n, \\ \dfrac{2mn(\cos(n\pi)\cos(m\pi) - 1)}{n^2 - m^2}, & \text{if } m \neq n, \end{cases}$$

$$g_{mn} = \int_0^1 Y_n''(\xi) Y_m(\xi)\,\mathrm{d}\xi = \begin{cases} -(n\pi)^2, & \text{if } m = n, \\ 0, & \text{if } m \neq n, \end{cases}$$

$$h_{mn} = \int_0^1 Z_n''(\xi) Z_m(\xi)\,\mathrm{d}\xi = \begin{cases} -(n\pi)^2, & \text{if } m = n, \\ 0, & \text{if } m \neq n, \end{cases}$$

$$i_{mn} = \int_0^1 Z_n'(\xi) Y_m(\xi)\,\mathrm{d}\xi = \begin{cases} -n\pi, & \text{if } m = n, \\ 0, & \text{if } m \neq n, \end{cases}$$

$$j_{mn} \int_0^1 Y_n'(\xi) Z_m(\xi)\,\mathrm{d}\xi = \begin{cases} n\pi, & \text{if } m = n, \\ 0, & \text{if } m \neq n, \end{cases}$$

$$k_{mni} = \int_0^1 Y_n'(\xi) Y_i''(\xi) Y_m(\xi)\,\mathrm{d}\xi = \begin{cases} -\dfrac{\sqrt{2}}{2} ni^2\pi^3, & \text{if } m = i \pm n, \\ \dfrac{\sqrt{2}}{2} ni^2\pi^3, & \text{if } m = n - i, \\ 0, & \text{others}, \end{cases}$$

$$l_{mnij} = \int_0^1 Y_n'(\xi) Y_i''(\xi) Y_j'(\xi) Y_m(\xi)\,\mathrm{d}\xi = \begin{cases} -\frac{1}{2} ni^2 j\pi^4, & \text{if } m = n + i \pm j,\ m = i - n \pm j, \\ \frac{1}{2} ni^2 j\pi^4, & \text{if } m = n - i \pm j,\ m = -n - i + j, \\ 0, & \text{others}. \end{cases}$$

APPENDIX C

The elements of matrices $\mathbf{M}$, $\mathbf{N}$, $\mathbf{\Phi}_\beta$, $\mathbf{B}$ and $\mathbf{U}$ are given as follows.

$$\mathbf{M} = \begin{bmatrix} M_{11} & M_{12} & M_{13} & \mathbf{M}_{14} & \mathbf{M}_{15} & \mathbf{M}_{16} \\ M_{21} & M_{22} & M_{23} & \mathbf{M}_{24} & \mathbf{M}_{25} & \mathbf{M}_{26} \\ M_{31} & M_{32} & M_{33} & \mathbf{M}_{34} & \mathbf{M}_{35} & \mathbf{M}_{36} \\ \mathbf{M}_{41} & \mathbf{M}_{42} & \mathbf{M}_{43} & \mathbf{M}_{44} & \mathbf{M}_{45} & \mathbf{M}_{46} \\ \mathbf{M}_{51} & \mathbf{M}_{52} & \mathbf{M}_{53} & \mathbf{M}_{54} & \mathbf{M}_{55} & \mathbf{M}_{56} \\ \mathbf{M}_{61} & \mathbf{M}_{62} & \mathbf{M}_{63} & \mathbf{M}_{64} & \mathbf{M}_{65} & \mathbf{M}_{66} \end{bmatrix}, \qquad \mathbf{N} = \begin{bmatrix} N_1 \\ N_2 \\ N_3 \\ \mathbf{N}_4 \\ \mathbf{N}_5 \\ \mathbf{N}_6 \end{bmatrix},$$

$$\mathbf{\Phi}_\beta = \begin{bmatrix} -\cos\phi \\ R\cos\theta \\ 0 \\ \mathbf{0} \\ \mathbf{0} \\ \mathbf{0} \end{bmatrix}^T, \qquad \mathbf{B} = [0 \quad -1 \quad 0 \quad \mathbf{0} \quad \mathbf{0} \quad \mathbf{0}]^T, \qquad \mathbf{U} = [I_q^*],$$

where $\mathbf{M}$ are the $(2+3m)\times(2+3m)$ matrices, $\mathbf{N}$ and $\mathbf{\Phi}_\beta^T$ are the $(2+3m)\times 1$ matrices, $M_{11}, M_{12}, M_{13}, M_{21}, M_{22}, M_{23}, M_{31}, M_{32}, M_{33}$ are chosen as the 1×1 matrices, $\mathbf{M}_{14}, \mathbf{M}_{15}, \mathbf{M}_{16}, \mathbf{M}_{24}, \mathbf{M}_{25}, \mathbf{M}_{26}, \mathbf{M}_{34}, \mathbf{M}_{35}, \mathbf{M}_{36}$ are chosen as the $1\times m$ matrices, $\mathbf{M}_{41}, \mathbf{M}_{42}, \mathbf{M}_{43}, \mathbf{M}_{51}, \mathbf{M}_{52}, \mathbf{M}_{53}, \mathbf{M}_{61}, \mathbf{M}_{62}, \mathbf{M}_{63}, \mathbf{N}_4, \mathbf{N}_5, \mathbf{N}_6$ are chosen as the $m\times 1$ matrices, $\mathbf{M}_{44}, \mathbf{M}_{45}, \mathbf{M}_{46}, \mathbf{M}_{54}, \mathbf{M}_{55}, \mathbf{M}_{56}, \mathbf{M}_{64}, \mathbf{M}_{65}, \mathbf{M}_{66}$ are chosen as the $m\times m$ matrices and

$$M_{11} = \Bigg[(h\sec^2\phi - 2h - 1)\,(S_4 + \tfrac{1}{3}) + \frac{1}{\sqrt{2}}\Bigg((h\sec^2\phi - 2(h+1)) \sum_{m=1}^{\infty} c_m f_m - 2h\tan\phi \sum_{m=1}^{\infty} c_m g_m \Bigg) - \tfrac{1}{2}\Bigg(\sum_{m=1}^{\infty} f_m^2 + \sum_{m=1}^{\infty} g_m^2 \Bigg) + \frac{\zeta^2}{2} \sum_{m=1}^{\infty} \Psi_m^2 + \zeta^2 - S_4\, h\sec^2\phi \times \Bigg((h\tan^2\phi - 1) - \frac{1}{\sqrt{2}} \sum_{m=1}^{\infty} a_m f_m \Bigg) \Bigg],$$

$$M_{12} = \Bigg[R((h+1)\cos(\theta+\phi) + h\tan\phi\sin(\theta+\phi))\,(S_4 + \tfrac{1}{2}) + \frac{R}{\sqrt{2}}\Bigg(\cos(\theta+\phi) \sum_{m=1}^{\infty} a_m f_m + \sin(\theta+\phi) \sum_{m=1}^{\infty} a_m g_m \Bigg) - S_4\, Rh\sec^2\phi\cos(\theta+\phi) \Bigg],$$

$$M_{13} = \Bigg[(S_4 + \tfrac{1}{3})\tan\phi + \frac{1}{\sqrt{2}}\Bigg(\tan\phi \sum_{m=1}^{\infty} c_m f_m - \sum_{m=1}^{\infty} c_m g_m \Bigg) - S_4\, h\sec^2\phi\tan\phi \Bigg],$$

$$\mathbf{M}_{14} = -\frac{1}{\sqrt{2}}\Bigg(\frac{1}{\sqrt{2}} \sum_{m=1}^{\infty} g_m + h\tan\phi \sum_{m=1}^{\infty} c_m \Bigg),$$

$$\mathbf{M}_{15} = \frac{1}{\sqrt{2}}\Bigg(\frac{1}{\sqrt{2}} \sum_{m=1}^{\infty} f_m + (1+h) \sum_{m=1}^{\infty} c_m - S_4\, h\sec^2\phi \sum_{m=1}^{\infty} a_m \Bigg),$$

$$\mathbf{M}_{16} = \mathbf{0},$$

$$M_{21} = \Bigg(\frac{R}{\sqrt{2}} \sum_{m=1}^{\infty} a_m g_m + R(S_4 + \tfrac{1}{2})h\tan\phi \Bigg)\sin(\theta+\phi) + \Bigg(-\frac{R}{\sqrt{2}} \sum_{m=1}^{\infty} a_m f_m - R(S_4 + \tfrac{1}{2})\,(h\tan^2\phi - 1) \Bigg)\cos(\theta+\phi),$$

$$M_{22} = [-R^2(S_4 + 1) - \tfrac{1}{3}\, S_2\, R^2 - \bar{J}_m],$$

$$M_{23} = [R(S_4 + \tfrac{1}{2})\,(\sin(\theta+\phi) + \tan\phi\cos(\theta+\phi))],$$

$$\mathbf{M}_{24} = \frac{R}{\sqrt{2}} \sum_{m=1}^{\infty} a_m \sin(\theta+\phi), \qquad \mathbf{M}_{25} = \frac{R}{\sqrt{2}} \sum_{m=1}^{\infty} a_m \cos(\theta+\phi), \qquad \mathbf{M}_{26} = 0,$$

$$M_{31} = h\tan\phi, \qquad M_{32} = -R\sin(\theta+\phi)\cos^2\phi, \qquad M_{33} = 1, \qquad \mathbf{M}_{34} = \mathbf{M}_{35} = \mathbf{M}_{36} = 0,$$

$$\mathbf{M}_{41} = g_m - \sqrt{2} c_m\, h\tan\phi, \qquad \mathbf{M}_{41} = g_m - \sqrt{2} c_m\, h\tan\phi,$$

$$\mathbf{M}_{42} = -\sqrt{2}a_m\, R \sin(\theta+\phi), \qquad \mathbf{M}_{43} = \sqrt{2}c_m, \qquad \mathbf{M}_{44} = 1, \qquad \mathbf{M}_{45} = \mathbf{M}_{46} = 0,$$

$$\mathbf{M}_{51} = -f_m + \sqrt{2}c_m\,(h\tan^2\phi - 1), \qquad \mathbf{M}_{52} = \sqrt{2}a_m\, R\cos(\theta+\phi),$$

$$\mathbf{M}_{53} = \sqrt{2}c_m \tan\phi, \qquad \mathbf{M}_{54} = 0, \qquad \mathbf{M}_{55} = 1, \qquad \mathbf{M}_{56} = 0,$$

$$\mathbf{M}_{61} = \mathbf{M}_{62} = \mathbf{M}_{63} = \mathbf{M}_{64} = \mathbf{M}_{65} = 0, \qquad \mathbf{M}_{66} = 1,$$

$$N_1 = \Bigg[S_4\, h\sec^2\phi\left(\frac{1}{\sqrt{2}}\sum_{m=1}^{\infty} a_m\, g_m - h\tan\phi(2\sec^2\phi - 1)\right) + 2h\sec^2\phi(\tan\phi(S_4 + \tfrac{1}{3})$$

$$+ \frac{1}{\sqrt{2}}\tan\phi\sum_{m=1}^{\infty} c_m f_m - \frac{1}{\sqrt{2}}\sum_{m=1}^{\infty} c_m\, g_m \Bigg]\dot{\phi}^2 + \Bigg[R(h\tan\phi\cos(\theta+\phi)$$

$$- (h+1)\sin(\theta+\phi))\,(S_4 + \tfrac{1}{2}) + \frac{R}{\sqrt{2}}\cos(\theta+\phi)\sum_{m=1}^{\infty} a_m\, g_m$$

$$- \frac{R}{\sqrt{2}}\sin(\theta+\phi)\sum_{m=1}^{\infty} a_m f_m + S_4\, Rh\sec^2\phi\sin(\theta+\phi)\Bigg]\dot{\theta}^2 + 2\Bigg[(S_4 + \tfrac{1}{3})\dot{h}\tan^2\phi$$

$$- \left(\frac{1}{\sqrt{2}}(h+1)\sum_{m=1}^{\infty} a_m \dot{f}_m - \frac{1}{\sqrt{2}}\dot{h}\tan^2\phi\sum_{m=1}^{\infty} c_m f_m\right.$$

$$\left. + \tan\phi\left(\frac{1}{\sqrt{2}}h\sum_{m=1}^{\infty} c_m\,\dot{g}_m + \frac{1}{\sqrt{2}}\dot{h}\sum_{m=1}^{\infty} a_m\, g_m\right)\right) - \tfrac{1}{2}\sum_{m=1}^{\infty} f_m\dot{f}_m - \tfrac{1}{2}\sum_{m=1}^{\infty} g_m\,\dot{g}_m$$

$$- S_4\, h\sec^2\phi\left(\dot{h}\tan^2\phi - \frac{1}{\sqrt{2}}\sum_{m=1}^{\infty} a_m\dot{f}_m\right)\Bigg]\dot{\phi} - \Bigg\{\frac{1}{\pi^4\eta^2}\Bigg(h\tan\phi - \sum_{m=1}^{\infty}(-1)^m\Psi_m$$

$$+ \sum_{m=1}^{\infty}(-1)^m(m\pi)g_m\Bigg) + \frac{1}{\pi^4\zeta^2}\Bigg[(h + \tfrac{3}{2}h^2\tan^2\phi)\sum_{m=1}^{\infty}(-1)^m(m\pi)g_m$$

$$+ h^2\tan\phi(\tfrac{1}{2}h\tan^2\phi + 1) + \Bigg(\sum_{m=1}^{\infty}\sum_{n=1}^{\infty}(-1)^{m+n}(mn\pi^2)f_n$$

$$+ \sum_{m=1}^{\infty}\sum_{n=1}^{\infty}(-1)^m(mn^2\pi^3)g_n^2\Bigg)g_m + h\tan\phi\Bigg(\sum_{m=1}^{\infty}(-1)^m(m\pi)f_m$$

$$+ \tfrac{3}{2}\sum_{m=1}^{\infty}(m\pi)^2 g_m^2\Bigg)\Bigg]\Bigg\}h\sec^2\phi,$$

$$N_2 = -\bar{B}_m\,\dot{\theta} + \Bigg[\sqrt{2}R\sum_{m=1}^{\infty} a_m\,\dot{g}_m\,\dot{\phi} - \frac{R}{\sqrt{2}}\sum_{m=1}^{\infty} a_m f_m\,\dot{\phi}^2 + R(2\dot{h}\dot{\phi}\tan\phi + (h-1)\dot{\phi}^2$$

$$+ 2h\dot{\phi}^2\sec^2\phi)\,(S_4 + \tfrac{1}{2})\Bigg]\sin(\theta+\phi) + \Bigg[\sqrt{2}\sum_{m=1}^{\infty} a_m\dot{f}_m\,\dot{\phi} + \frac{1}{\sqrt{2}}\sum_{m=1}^{\infty} a_m\,g_m\,\dot{\phi}^2$$

$$- 2R\dot{h}\dot{\phi}\tan^2\phi(S_4+\tfrac{1}{2}) - R\tan\phi(2\sec^2\phi - 1)\,(S_4+\tfrac{1}{2})\dot{\phi}^2\Bigg]\cos(\theta+\phi)$$

$$N_3 = 2\dot{\phi}\dot{h}\tan\phi + \frac{1}{\pi^4\eta^2}\frac{1}{S_4}\cos^2\phi\tan\phi\Bigg[\sum_{n=1}^{\infty}(n\pi)\,(-1)^n g_n - \sum_{n=1}^{\infty}(-1)^n\Psi_n\Bigg]$$

$$+ h\Bigg\{(2\sec^2\phi - 1)\dot{\phi}^2 + \frac{1}{\pi^4\eta^2}\frac{1}{S_4}\sin^2\phi + \frac{1}{\pi^4\zeta^2}\frac{1}{S_4}\cos^2\phi$$

$$\times\Bigg[1 + 2\sum_{n=1}^{\infty}(n\pi)\,(-1)^n g_n\tan\phi$$

$$+ \tfrac{3}{2}\sum_{n=1}^{\infty}\sum_{i=1}^{\infty}(i\pi)\,(n\pi)\,(-1)^{n+i} g_i\,g_n\tan^2\phi + \sum_{n=1}^{\infty}(n\pi)\,(-1)^n f_n\tan^2\phi\Bigg]\Bigg\}$$

$$+ \frac{1}{\pi^4\zeta^2}\frac{1}{S_4}\cos^2\phi\Bigg\{\tfrac{1}{2}h^3\tan^4\phi + \tfrac{3}{2}h^2\tan^2\phi\Bigg[1 + \sum_{n=1}^{\infty}(n\pi)\,(-1)^n g_n\tan\phi\Bigg]$$

$$+ \Bigg[\sum_{n=1}^{\infty}(n\pi)\,(-1)^n f_n + \tfrac{1}{2}\sum_{n=1}^{\infty}\sum_{i=1}^{\infty}(i\pi)\,(n\pi)\,(-1)^{n+i} g_i\,g_n\Bigg]$$

$$\times\Bigg[1 + \sum_{n=1}^{\infty}(n\pi)\,(-1)^n g_n\tan\phi\Bigg]\Bigg\} - R\dot{\theta}^2\cos(\theta+\phi)\cos^2\phi - \dot{\phi}^2 - \frac{1}{S_4}\bar{F}\cos\phi,$$

$$\mathbf{N}_4 = \epsilon_1\dot{f}_m + 2\dot{\phi}\dot{g}_m + \sqrt{2}c_m\,\epsilon_1\,\dot{h} - \dot{\phi}^2 f_m + \frac{1}{\pi^4\zeta^2}\Bigg[(m\pi)^2 f_m - \sum_{n=1}^{\infty}\sum_{i=1}^{\infty} k_{mni}\,g_i\,g_n$$

$$+ (m\pi)^2 h\tan\phi g_m\Bigg] + \sqrt{2}\{c_m\,[2\dot{h}\dot{\phi}\tan\phi - h\dot{\phi}^2(1 - 2\sec^2\phi) - \dot{\phi}^2]$$

$$- Ra_m\,\dot{\theta}^2\cos(\theta+\phi)\},$$

$$\mathbf{N}_5 = \epsilon_2\,\dot{g}_m + \sqrt{2}c_m\,\epsilon_2\tan\phi\dot{h} - 2\dot{\phi}\dot{f}_m - \dot{\phi}^2 g_m + \frac{1}{\pi^4\eta^2}((m\pi)^2 g_m - (m\pi)\Psi_m)$$

$$- \frac{1}{\pi^4\zeta^2}\Bigg[\frac{1}{\sqrt{2}}\sum_{n=1}^{\infty}\sum_{i=1}^{\infty} k_{mni}\,f_i\,g_n - (m\pi)^2 h\tan\phi f_m + \tfrac{3}{2}\Bigg(\tfrac{1}{2}\sum_{n=1}^{\infty}\sum_{i=1}^{\infty}\sum_{j=1}^{\infty} l_{mnij}\,g_j\,g_i\,g_n$$

$$+ \frac{2}{\sqrt{2}}h\tan\phi\sum_{n=1}^{\infty}\sum_{i=1}^{\infty} k_{mni}\,g_i\,g_n - (m\pi)^2 h^2\tan^2\phi g_m\Bigg) + \frac{1}{\sqrt{2}}\sum_{n=1}^{\infty}\sum_{i=1}^{\infty} k_{mni}\,g_i f_n$$

$$- h(m\pi)^2 g_m \Big] + \sqrt{2}\,\{c_m\,[2\dot{h}\dot{\phi}\,\tan^2\phi + h(\epsilon_2\,\dot{\phi}\,\sec^2\phi - \dot{\phi}^2\tan\phi(1 - 2\sec^2\phi))]$$

$$- Ra_m\,\dot{\theta}^2\sin(\theta + \phi)\},$$

$$\mathbf{N}_6 = \frac{\epsilon_2}{\zeta^2}\,\dot{\Psi}_m + \left(\frac{1}{\pi^4\eta^2\zeta^2} - \dot{\phi}^2 + \frac{1}{\pi^4\zeta^2}(m\pi)^2\right)\Psi_m - \frac{1}{\pi^4\eta^2\zeta^2}(m\pi)g_m,$$

APPENDIX D

Choose $\mathbf{p} = [\phi]$, $\mathbf{q} = [\theta\ \ h\ \ \mathbf{f}\ \ \mathbf{g}\ \ \mathbf{\Psi}]$, $\mathbf{\Phi}_q = [R\cos\theta\ \ 0\ \ \mathbf{0}\ \ \mathbf{0}\ \ \mathbf{0}]$ and $\mathbf{\Phi}_p = [-\cos\phi]$. The entries of matrices in equation (36) are

$$\mathbf{M}^{pp} = [\mathbf{M}_{11}], \quad \mathbf{M}^{pq} = [M_{12}\ \ M_{13}\ \ \mathbf{M}_{14}\ \ \mathbf{M}_{15}\ \ \mathbf{M}_{16}],$$

$$\mathbf{M}^{qp} = [M_{21}\ \ M_{31}\ \ \mathbf{M}_{41}\ \ \mathbf{M}_{51}\ \ \mathbf{M}_{61}]^T, \qquad \mathbf{M}^{qq} = \begin{bmatrix} M_{22} & M_{23} & \mathbf{M}_{24} & \mathbf{M}_{25} & \mathbf{M}_{26} \\ M_{32} & M_{33} & \mathbf{M}_{34} & \mathbf{M}_{35} & \mathbf{M}_{36} \\ \mathbf{M}_{42} & \mathbf{M}_{43} & \mathbf{M}_{44} & \mathbf{M}_{45} & \mathbf{M}_{46} \\ \mathbf{M}_{52} & \mathbf{M}_{53} & \mathbf{M}_{54} & \mathbf{M}_{55} & \mathbf{M}_{56} \\ \mathbf{M}_{62} & \mathbf{M}_{63} & \mathbf{M}_{64} & \mathbf{M}_{65} & \mathbf{M}_{66} \end{bmatrix},$$

$$\mathbf{N}^p = [N_1], \qquad \mathbf{N}^q = [N_2\ \ N_3\ \ \mathbf{N}_4\ \ \mathbf{N}_5\ \ \mathbf{N}_6]^T, \qquad \mathbf{B}^p = [0].$$

Where the elements (e.g., $M_{11}, M_{12}, \ldots, \mathbf{M}_{66}, N_1, N_2, \ldots, \mathbf{N}_6$) are the same as in Appendix B.

APPENDIX E: NOMENCLATURE

A	cross-sectional area of the connecting rod
B_m	motor damping coefficient
$\mathbf{C}_1$, $\mathbf{C}_2$	gain matrices for the switching function of the speed control
$\mathbf{C}_i$, $\mathbf{C}_j$	gain matrices for the switching function of the tracking control
C_x, C_y, C_ψ	coefficients for viscous damping
d	flexible connecting rod diameter
E	Young's modulus
$\mathbf{e}$	the speed error vector for the speed controller
$\tilde{\mathbf{e}}_i$	the position error vector for the tracking controller
$\tilde{\mathbf{e}}_j$	the speed error vector for the tracking controller
$\mathbf{e}_i$, $\mathbf{e}_j$	unit vectors in the x and y directions, respectively
$\mathbf{e}_r$, $\mathbf{e}_\theta$	unit vectors of the rotation co-ordinates originated at O
F	external force acting on the slider
F^C	the generalized constraint reaction force
g_r	gear ratio
$h(\tau)$	non-dimensional axial deformation of the connecting rod at $\xi = 1$
I	area moment of inertia about the neutral axis
$\mathbf{i}$, $\mathbf{j}$	unit vectors in the X and Y directions, respectively
I_q^*	non-dimensional input current
i_q^*	q-axis current
J_m	motor moment inertia
K	shear deflection coefficient
K_T	motor torque constant
l	length of connecting rod
M_2, M_4	mass of crank and slider, respectively
N	reaction force
P, Q	positive constant coefficient

$\mathbf{Q}$	the vector of generalized co-ordinates
r	length of the crank
R	dimensionless crank length
$\mathbf{R}$	position vector related to XOY co-ordinate system
S	switching function
sgn (S)	sign function
sat (S)	saturation function
T_2	the kinetic energy of the crank
T_3	the kinetic energy of the flexible connecting rod
T_4	the kinetic energy of the slider
t	time
$\mathbf{U}$	control input
U_3	the strain energy of the flexible connecting rod
u, v	longitudinal and transverse displacements of the rod, respectively
xAy	moving co-ordinate system
XOY	global co-ordinate system
Δ	boundary layer width
$\mathbf{\Phi}_Q$	holonomic constraint equation
Λ	Lagrange multiply
$\epsilon_{xx}, \epsilon_{xy}, \epsilon_{yy}$	Lagrangian strains
ϕ	angle between X-axis and undeformed axis of the flexible connecting rod
κ	constant coefficient between 0 and 1
μ	the coefficient of sliding friction
θ	crank angle
ρ	mass density of connecting rod
τ	dimensionless time
τ_a	torque applying to the crank
τ_m	motor torque
ξ	dimensionless crank length parameter
ψ	the slope of the deflection curve due to bending deformation alone